NASA TN D-301

TECHNICAL NOTE

D-301

SPATIAL CHARACTERISTICS OF WATER SPRAY FORMED BY TWO IMPINGING JETS AT SEVERAL JET VELOCITIES IN QUIESCENT AIR

By Hampton H. Foster and Marcus F. Heidmann

Lewis Research Center
Cleveland, Ohio

NATIONAL AERONAUTICS AND SPACE ADMINISTRATION

WASHINGTON

July 1960

NATIONAL AERONAUTICS AND SPACE ADMINISTRATION

TECHNICAL NOTE D-301

SPATIAL CHARACTERISTICS OF WATER SPRAY FORMED BY TWO IMPINGING JETS AT SEVERAL JET VELOCITIES IN QUIESCENT AIR

By Hampton H. Foster and Marcus F. Heidmann

SUMMARY

The spatial characteristics of a spray formed by two impinging water jets in quiescent air were studied over a range of nominal jet velocities of 30 to 74 feet per second. The total included angle between the 0.089-inch jets was 90°. The jet velocity, spray velocity, disappearance of the ligaments just before drop formation, mass distribution, and size and position of the largest drops were measured in a circumferential survey around the point of jet impingement. Photographic techniques were used in the evaluations.

The distance from the point of jet impingement to ligament breakup into drops was about 4 inches on the spray axis and about 1.3 inches in the radial position ±90° from the axis. The distance tended to increase slightly with increase in jet velocity.

The spray velocity varied from about 99 to about 72 percent of the jet velocity for a change in circumferential position from the spray axis to the ±80° positions. The percentages tended to increase slightly with an increase in jet velocity. Fifty percent of the mass was distributed about the spray axis in an included angle of slightly less than 40°. The effect of jet velocity was small.

The largest observed drops (2260-micron or 0.090-in. diam.) were found on and about the spray axis. The size of the largest drops decreased for an increase in radial angular position, being about 1860 microns (0.074 in.) at the ±90° positions. The largest drop sizes tended to decrease for an increase in jet velocity, although the velocity effect was small.

A drop-size distribution analysis indicated a mass mean drop size equal to 54 percent of an extrapolated maximum drop size.

The spray properties were analyzed for correlating parameters. Sheet length at breakup and a calculated apparent sheet thickness were found to vary nearly proportionally with the square root of the ratio of mass-flow rate to spray velocity in a spray-pattern sector. Maximum drop size decreased with sheet thickness; however, no functional relation could be established because of the scatter in data.

INTRODUCTION

The spray pattern produced by two impinging jets is primarily two-dimensional in a plane perpendicular to the plane of the jets. The spray is formed by flow which propagates approximately radially from the point of jet impingement. This radial flow is not circumferentially uniform. Consequently, spatial variations in the spray pattern exist. Although such sprays have been studied extensively, most investigators treat the spray as a unit and report single-value properties for the entire spray as in references 1 and 2. Spatial variations are reported in reference 3; however, only a limited number of such studies have been made.

The purpose of this study was twofold: (1) to provide additional data on spatial characteristics, and (2) to provide data on a specific atomizer which has been used in experimental combustion tests. Such data would be an aid in mathematical analysis of spray formation and in interpreting combustion phenomena in the vicinity of the injector. Specifically, the maximum drop size, mass flow, liquid-sheet breakup characteristics, and spray velocity were measured along radial paths leading from the point of impingement. These measurements were made on water sprays, in quiescent air, with an atomizer having a pair of 0.089-inch-diameter impinging jets with a total included angle of 90°. This atomizer was used in rocket-engine combustion tests reported in references 4 to 6. A jet-velocity range similar to that used in the combustor tests was investigated; these velocities included values typical of those encountered in current rocket-engine design practice.

APPARATUS AND PROCEDURE

The atomizer details are shown in figure 1(a). In combustor tests this atomizer was used for like-on-like impingement of a variety of liquid propellants. In the present spray studies water was used and the spatial spray characteristics were obtained for a jet-velocity range of 30 to 74 feet per second. In all cases the sprays were formed in quiescent air.

The flow system used is shown schematically in figure 1(b). The water tank pressure was limited to 100 pounds per square inch. The

water-flow rate was measured with a recording flowmeter. The spray axis was horizontal, and the spray plane was normal to the horizontal plane in all tests. Shadowgraph pictures of the spray ligaments and drops were obtained with a 35-millimeter camera using single flashes of a microflash light source (fig. 1(c)); an example is shown in figure 2.

Figure 2 also shows the layout of the clear plastic mask placed over the spray shadowgraphs to determine the positions of the ligaments and drops. The 35-millimeter film (shadowgraph record) was viewed with a device which afforded a fivefold magnification of the spray particles and also vertical and horizontal movable crosshairs with suitable scales for measuring drop diameters. Five pictures were obtained for each jet velocity to minimize random variations. Only the three largest drops in each 10° sector were measured and used in the analysis; these data are listed in table I. (Blank spaces in the table indicate data not available.)

The distance from the point of jet impingement to complete breakup of the ligaments was also obtained from the pictures. The sheet breakup distance was not directly discernable for many of the flow conditions used; a definite spray property was needed to indicate this liquid-sheet characteristic. The position at which circumferentially alined ligaments disappeared with respect to the point of jet impingement was discernable, and this position was assumed as an index of sheet length. This radial distance was measured in each 10° angular increment in the five photographs for each jet velocity. Where sheet breakup distance was measurable it was equal to about one-half the distance for complete ligament breakup.

Photomicrographs of the spray were obtained with a large box camera arrangement shown schematically in figure 1(d). The photomicrographs were obtained at 1, 2, 3, 4, 5, and 6 inches laterally displaced above the horizontal spray axis 8 inches downstream from the atomizer. A jet velocity of 60 feet per second was used for these photomicrographs. One photomicrograph at each of the foregoing positions, however, was analyzed to provide a qualitative picture of the drop-size distribution. Each photomicrograph provided a spray sample of about 100 drops (table II).

Spray-velocity measurements were made by a streak-photograph technique (fig. 1(e)). Velocity data were obtained along the spray axis and also along the 20°, 40°, 60°, and 80° positions for each of the four jet velocities. Velocity of a single jet was also measured. Spray or jet velocity is computed as the product of the film speed, the tangent of the average streak angle, and the proper scale factor.

Values of jet velocity obtained from film data were compared with values of jet velocity calculated from measurements of flow and tube cross-sectional area.

Mass distribution within the spray was measured with a collector divided into five 20° sectors (fig. 1(f)). The spray pattern was assumed to be symmetrical about the spray axis in the vertical plane; therefore the spray collection was obtained in only one quadrant as indicated.

RESULTS

Spray Photographs

Photographs of the overall spray pattern at nominal jet velocities of 30, 60, and 74 feet per second are shown in figure 3. The process of disintegration appears similar throughout this velocity range.

Jet Velocity

Values of jet velocity determined from streaked-moving-film records are shown in figure 4 for a range of jet velocities. Data are shown for two downstream positions, near the jet origin and 5 to 8 inches downstream. Velocities from the film data are plotted against the velocities calculated from flow-rate measurements for comparison. Flow rates were accurate to within ±1 percent. The accuracy of the streak-photography measurements is not readily defined, but is estimated to be within ±2 percent. Although the departure from the theoretical value increases slightly with increase in jet velocity, the two methods of jet-velocity determination are in agreement within measurement accuracy. The results indicate that no significant contraction or expansion of the jet occurs at the tube outlet. Jet velocity calculated from flow rate was, therefore, used as a basis for comparison of the spray velocities.

Spray Velocity

Figure 5 shows the effect of jet velocity on spray velocity for several angular positions about the spray axis. These evaluations were made in the region 3 to 4 inches from the impingement point of the jets. They show that spray velocity varies nearly proportionately with jet velocity. A cross plot of these data is shown in figure 6; that is, the ratio of spray to jet velocity is presented as a function of angular position about the spray axis. As could be expected, the highest ratios (93 to 99 percent) occur along the spray axis. This ratio decreases to a minimum of 72 to 77 percent at the 80° positions.

Mass Distribution

Mass distribution is shown in figure 7. The tops of the shaded rectangles represent the average for the four jet velocities. The

experimental results shown are average values of repeated tests. The effect of jet velocity appears to be within experimental accuracy. The data plot indicates that about 50 percent of the total spray mass is accounted for in an angular sector of 40° equally spaced about the spray axis.

Breakup of Liquid Sheets into Ligaments

An analysis of spray photographs (similar to those in fig. 2) was made to determine the radial distance and angular position for complete breakup into drops. Figure 8 shows a plot of the mean value of distance to breakup obtained from five photographs for each of the four jet velocities investigated. The longest travel of the liquid sheet before breakup into ligaments and finally into drops occurs at the spray axis. The distance diminishes gradually until at right angles to the spray axis the distance is about one-third to one-fourth that along the spray axis, that is, 1.3 compared with 4 inches. The effect of spray velocity on distance of breakup is not pronounced. However, there is a slight increase in distance for an increase in jet velocity at the spray axis.

Maximum Drop Size

Table I lists the three largest drops in focus in each 10° sector as read from the shadowgraphs and their respective positions with respect to the spray axis and the point of jet impingement. High-speed photographs for transient conditions showed that these large drops form during ligament disintegration and once formed do not change in size. A limiting drop size may repeatedly occur in a sector if drop stability is such that all drops larger than a critical size disintegrate. The data, however, indicate that size distribution and probability affect the measurements made. Measured maximum drop sizes appear to decrease with an increase in jet velocity and with an increase in angular position with respect to the spray axis. The maximum sizes listed in table I are between 0.036 and 0.090 inch in diameter.

Drop-Size Distribution

A log probability plot of the drop-size measurements obtained from photomicrographs (table II) is shown in figure 9(a). The pictures were taken 8 inches downstream from the atomizer, that is, sufficiently far from the point of jet impingement for complete breakup (ref. 1). The data are typical of impinging-jet sprays in that the distribution tends to terminate at a finite maximum drop size in the large-drop-size region.

DISCUSSION

The results obtained for spray velocity, mass distribution, and disappearance of circumferentially alined ligaments are comparatively self-descriptive and in many respects characterize the spray formed by the impingement of twin jets. The data on measured maximum drop size, however, require further analysis if they are to be used as a spray characteristic. The following discussion entails an analysis of these data combined with previously reported data for impinging-jet injectors of similar design. The spray characteristics will then be analyzed for possible interrelation.

In reference 1 drop-size data were obtained from impinging-jet sprays for three jet diameters and for various jet velocities and surrounding air velocities. These data were obtained for heptane sprays where each spray sample contained about 1000 drops. The data were analyzed for mean drop size using the Nukiyama-Tanasawa drop-size-distribution expression (refs. 7 and 8). These data also fit an "upper-limit" expression (ref. 8) for drop-size distribution. The "upper limit" expression is the same as the log-probability expression

$$\frac{dR}{dy} = \frac{\delta}{\sqrt{\pi}} e^{-\delta^2 y^2}$$

except that

$$y = \ln \frac{D}{D_m - D}$$

rather than

$$y = \ln \frac{D}{\overline{D}}$$

where R is the cumulative volume in percent, δ and $\overline{D}$ are constants, D is drop diameter, and D_m is a maximum drop diameter.

The "upper-limit" expression is based on the premise that distribution terminates at a finite maximum drop size. Reference 8 discusses methods of obtaining a mean drop diameter such as D_{30}, D_{31}, and D_{32} from plots such as shown in figure 10.

Figure 9(b) shows a typical log-probability plot of data from reference 1; a curved line is almost always obtained. The curve may be extrapolated to obtain a value for D_m, and the parameter $D/(D_m - D)$ may be evaluated.

Figure 10(a) shows a plot of all the data in reference 1 evaluated on the basis of this "upper-limit" expression for drop-size distribution. The data fall within about ±20 percent of a mean-value straight line. The mass mean for the straight line shown occurs at a value of $D/(D_m - D) = 1.17$, and the value of D/D_m is 0.54.

The drop-distribution data obtained in this study (fig. 9(a) and table II) may be similarly evaluated on the basis of the "upper-limit" expression for distribution. Figure 10(b) shows this plot. A straight line may again be used to approximate the data; however, the slope and position of the line differ from those of figure 10(a). The drop count for the data in reference 1 was about 1000 for each sampling, whereas the drop count for the data in this study was only 100 per sample. It has been observed that, where drop counts of 100 and 1000 are taken from a given spray sample and the "upper-limit" evaluation is used, the most probable straight line in the plot with the smaller number of data points will have a steeper slope and be displaced to the left of the straight line with the greater number of data points. This result is consistent with other statistical analyses of the effect of sample size on deviations in means. Differences in figures 10(a) and (b) may, therefore, be partially attributed to sample size.

Figure 10 indicates that drop-size distribution from impinging jets can be approximated by a single straight line from the "upper-limit" plot of the data. With this assumption, it is necessary only to establish a maximum drop size in order to approximate the entire distribution for the conditions considered.

As a means of obtaining an extrapolated value of the maximum drop diameter from the large-drop measurements (table I) a log-probability plot of a chosen range of D_m values and corresponding values of $D/(D_m - D)$ and R from figure 10(a) was prepared as shown in figure 11. As an example, the data points shown are from table I (jet velocity, 44 ft/sec; angular position, 50°). Values of ΔR are plotted against D, where

$$\Delta R = \frac{\frac{\rho \pi n D^3}{6}}{\sum \frac{\rho \pi n D^3}{6}}$$

(ρ is water density and n is number of drops of diameter D) and where equivalent values of $\sum \frac{\rho \pi n D^3}{6}$ were calculated from the experimental mass-distribution data shown in figure 7, the velocity characteristics from figure 6, and the radial length of spray elements analyzed in the spray photographs. In most cases the three large drops

represented about 5 to 30 percent of the mass in the sector considered. Extrapolation of these data to a nominal 100-percent R indicates a maximum drop size of about 2000 microns for the particular conditions considered. Maximum drop sizes were obtained in a similar manner for all spray sectors and jet velocities. The results are shown in figure 12 as a function of angular position for each jet velocity.

Figure 12 shows that extrapolated maximum drop sizes occur on or near the spray axis with a trend toward smaller maximum sizes with an increase in jet velocity. Maximum drop sizes, however, vary only between about 1800 and 2400 microns. Assuming the generalized distribution function shown in figure 10(a) to be valid, that is, $D/D_m = 0.54$, the mass mean drop diameter would show a variation of 970 to 1300 microns. The water-spray results are in relatively good agreement with those for heptane sprays (ref. 1), if the heptane data are corrected for the difference in surface tension and the difference in environmental test conditions is considered. If the foregoing correction is made, a maximum diameter of 1770 microns is calculated from reference 1 for water at conditions nearly comparable with those of this study.

Thus far in this study spray velocity, mass-flow rate, sheet breakup distance, and maximum drop size have been presented as a function of angular position in the spray pattern. The interrelation of these parameters is also of interest in describing spray characteristics in a more generalized form.

One combination of parameters which may show interrelations is velocity, mass-flow rate, and length of the unbroken liquid sheet. Inspection of the data has indicated a proportional relation between sheet length at breakup and the square root of the ratio of mass-flow rate to spray velocity. Figure 13 shows this correlation. Although appreciable scatter of data is evident, correlations based on only single functional relations appeared justified because of the statistical nature and limited range of the data.

Knowing the velocity, mass-flow rate, and sheet breakup length in a particular spray sector, one can calculate an apparent sheet thickness, where the apparent thickness is proportional to the mass flow divided by the sheet length and spray velocity. Since the length showed an approximate correlation with the ratio of mass flow to velocity, the apparent thickness can be similarly correlated.

Figure 14 shows such an apparent thickness as a function of the square root of the ratio of mass-flow rate to spray velocity. Apparent thickness varies between 0.0016 and 0.0046 inch or 40 and 115 microns.

The sheet thickness was considered as a probable property which governs drop-size distribution. An extrapolated maximum drop diameter is presented in figure 12 as an index of drop-size distribution. These maximum drop sizes are shown as a function of apparent sheet thickness in figure 15. A functional relation cannot be justified because of the scatter in data; however, the data imply that drop size is proportional to some small fractional power of sheet thickness.

The interrelations presented in this study are based on a relatively small range in several parameters. They require justification with additional experimental evidence to be generally applicable. The approach used has been one in which a spray sector is considered an entity in itself regardless of its source. Whether liquid-sheet disintegration can be studied in this manner or whether perturbations in internal energy and other factors are overriding effects remains to be evaluated. A similar study for other jet diameters would extend the range in parameters, and it appears to be the most fruitful approach to establishing more precise interrelations of spray-sector properties.

SUMMARY OF RESULTS

A study of the spray formed by two 0.089-inch-diameter impinging water jets in quiescent air for a nominal jet-velocity range of 30 to 74 feet per second showed the following spatial characteristics:

1. The resultant spray velocity varied between 72 and 99 percent of jet velocity in a circumferential survey around the point of impingement. Maximum and minimum velocities occurred along the spray axis and normal to the spray axis, respectively.

2. The disappearance of circumferentially alined ligaments was used as an indication of sheet breakup distance. The distance from the point of impingement varied between 4 and 1.3 inches. Maximum distances occurred along the spray axis. The effect of jet velocity was small, although there was a slight increase in distance for an increase in jet velocity.

3. Fifty percent of the mass was distributed in an angular increment of 40° centered about the spray axis. The effect of jet velocity was small.

4. A sampling of large-diameter drops showed that drop diameters approaching the jet diameter exist throughout the major portion of the spray.

5. Drop-size data from several impinging-jet injectors were analyzed using an "upper-limit" expression for size distribution. The

expression is based on the existence of a maximum drop diameter. Data for a variety of conditions were found to fit a single curve to within ±20 percent. The curve indicated a mass mean drop size equal to 54 percent of the maximum extrapolated drop size.

6. Large-drop sampling data were extrapolated for a maximum drop size on the basis of the average distribution curve. Maximum drop sizes from 1800 to 2400 microns were obtained. The largest values occurred along the spray axis.

7. The spray properties were analyzed for correlating parameters. Sheet breakup distance and a calculated apparent sheet thickness at breakup were found to be nearly proportional to the square root of the ratio of mass-flow rate to spray velocity. Maximum drop size increased with an increase in apparent sheet thickness; however, the data were too scattered to establish a functional relation.

Lewis Research Center
National Aeronautics and Space Administration
Cleveland, Ohio, May 6, 1960

REFERENCES

1. Ingebo, Robert D.: Drop-Size Distribution for Impinging-Jet Breakup in Airstreams Simulating the Velocity Conditions in Rocket Combustors. NACA TN 4222, 1958.

2. Heidmann, Marcus F., Priem, Richard J., and Humphrey, Jack C.: A Study of Sprays Formed by Two Impinging Jets. NACA TN 3835, 1957.

3. Rupe, Jack H.: A Technique for the Investigation of Spray Characteristics of Constant Flow Nozzles. Third Symposium on Combustion and Flame and Explosion Phenomena, The Williams & Wilkins Co., 1949, pp. 680-694.

4. Heidmann, M. F.: Propellant Vaporization as a Criterion for Rocket-Engine Design; Experimental Effect of Fuel Temperature on Liquid-Oxygen - Heptane Performance. NACA RM E57E03, 1957.

5. Clark, Bruce J., Hersch, Martin, and Priem, Richard J.: Propellant Vaporization as a Criterion for Rocket-Engine Design; Experimental Performance, Vaporization, and Heat-Transfer Rates with Various Propellant Combinations. NASA MEMO 12-29-58E, 1959.

6. Heidmann, Marcus F.: Propellant Vaporization as a Criterion for Rocket-Engine Design; Experimental Effect of Chamber Diameter on Liquid Oxygen - Heptane Performance. NASA TN D-65, 1959.

7. Bevans, Rowland S.: Mathematical Expressions for Drop Size Distribution in Sprays. Conf. on Fuel Sprays, Univ. Mich., Mar. 30-31, 1949.

8. Mugele, R. A., and Evans, H. G.: Droplet-Size Distribution in Sprays. Ind. and Eng. Chem., vol. 43, no. 6, June 1951, 1317-1324.

TABLE I. - DROP DIAMETERS AND RADIAL POSITIONS OF THREE LARGEST DROPS IN EACH SPRAY SECTOR OBTAINED FROM SHADOWGRAPH RECORDS

[Spray axis horizontal.]

35 millimeter picture frame	Drop diameter, in. / Distance from impingement point, in. — Angular position, deg																	
	Above spray axis									Below spray axis								
	90	80	70	60	50	40	30	20	10	10	20	30	40	50	60	70	80	90
Jet velocity, 30 ft/sec																		
1	0.052	0.056	0.066	0.042	0.060	0.064	0.064	0.068	0.072	0.080	0.062	0.068	0.068	0.040	0.066	0.052	0.050	0.040
	3.4	3.5	4.0	4.1	3.4	5.4	4.4	5.6	6.4	3.6	8.0	4.8	7.6	5.5	4.4	2.6	4.1	1.9
				0.050	0.062	0.066	0.066	0.070	0.074	0.082	0.070	0.072	0.080	0.066	0.068	0.060	0.054	0.046
				3.5	4.3	3.5	4.7	7.4	6.8	5.6	7.6	5.4	4.2	5.2	3.8	4.3	3.4	2.5
				0.054	0.062	0.072	0.066	0.078	0.080	0.090	0.072	0.072	0.080	0.070	0.070	0.068	0.064	0.050
				3.6	4.0	4.3	6.0	7.1	5.5	5.1	6.4	6.0	6.4	4.3	4.7	3.5	4.1	1.0
2	0.066	0.074	0.060	0.048	0.046	0.062	0.070	0.064	0.072	0.062	0.060	0.058	0.052	0.060	0.058	0.050	0.056	0.046
	3.5	3.8	2.3	5.0	5.0	5.5	5.2	5.4	4.8	7.7	6.5	6.6	4.8	5.5	4.0	3.8	2.3	2.1
				0.054	0.070	0.086	0.076	0.068	0.078	0.066	0.062	0.066	0.058	0.070	0.064	0.060	0.056	
				6.1	3.9	5.2	4.3	7.3	7.5	7.8	5.8	4.3	5.5	5.5	4.5	3.9	3.3	
					0.080	0.090	0.084	0.070	0.080	0.082	0.066	0.094	0.032	0.080	0.072		0.074	
					4.6	4.6	5.7	5.8	7.7	7.2	7.3	7.0	4.6	4.2	2.6		3.2	
3	0.048	0.054	0.056	0.054	0.048	0.054	0.052	0.068	0.066	0.060	0.054	0.062	0.048	0.072	0.040	0.060	0.060	0.060
	2.3	4.5	3.5	5.0	6.5	6.0	5.0	5.6	4.5	5.8	7.6	4.5	6.5	3.9	4.7	2.4	2.7	4.5
	0.048	0.054	0.056	0.066	0.056	0.072	0.062	0.074	0.070	0.060	0.062	0.072	0.066	0.072	0.060	0.060	0.062	0.064
	2.3	4.5	3.5	8.0	4.5	4.5	4.8	7.0	5.5	7.3	5.7	5.1	5.3	6.4	4.2	2.3	4.0	2.4
		0.056	0.058	0.074	0.062	0.072	0.064	0.076	0.090	0.074	0.074	0.074						
		2.7	2.6	3.0	4.2	4.5	5.5	6.5	6.5	5.9	5.1	8.2						
4	0.040	0.038	0.040	0.046	0.050	0.060	0.060	0.068	0.070	0.060	0.060	0.060	0.052	0.050	0.048	0.048	0.056	0.042
	2.3	2.3	4.2	3.8	5.3	5.3	7.6	5.3	5.5	6.0	8.0	4.5	3.5	4.9	3.2	3.0	3.0	3.0
	0.040	0.038	0.054	0.060	0.050	0.062	0.062	0.072	0.074	0.062	0.060	0.060	0.058	0.050	0.052	0.050	0.056	0.042
	2.7	2.3	3.2	4.7	6.3	4.5	6.5	7.0	6.9	7.5	7.5	5.4	4.5	7.0	4.3	4.8	4.5	3.0
	0.040	0.046		0.060	0.060	0.066	0.062	0.080	0.076	0.064	0.074	0.060	0.058	0.052	0.056	0.052	0.064	0.062
	3.5	2.6		5.5	3.4	5.5	6.5	5.3	6.7	6.8	4.7	5.7	7.3	5.7	4.3	4.8	3.3	3.5
5	0.020	0.031	0.027	0.050	0.054	0.062	0.058	0.068	0.070	0.050	0.060	0.056	0.058	0.056	0.044	0.048	0.050	0.044
	3.0	3.7	4.9	4.1	3.3	3.4	7.0	5.3	5.5	7.6	6.5	5.0	6.4	6.5	3.5	4.4	4.1	4.1
				0.058	0.054	0.072	0.068	0.072	0.074	0.070	0.060	0.060	0.062	0.060	0.046	0.056		
				2.4	5.5	5.2	5.6	7.0	6.9	6.5	7.5	6.5	6.4	5.5	5.4	4.3		
				0.060	0.070	0.072	0.072	0.080	0.076	0.074	0.062	0.070	0.064	0.064	0.050			
				3.9	4.4	5.3	4.3	5.3	6.7	4.4	7.5	7.2	7.8	6.0	4.5			
Jet velocity, 44 ft/sec																		
6		0.058	0.054	0.042	0.044	0.042	0.050	0.062	0.058	0.050	0.052	0.042	0.046	0.048	0.050	0.050	0.044	
		2.8	3.0	3.8	4.8	5.0	6.8	7.6	7.1	7.4	4.7	6.8	4.2	5.5	5.3	4.8	3.5	
				0.060		0.060	0.054	0.064	0.058	0.060	0.054	0.050	0.052					
				4.5		7.2	4.9	6.4	7.4	5.4	6.3	5.2	3.5					
						0.064	0.068	0.068	0.060	0.062	0.056	0.056	0.052					
						5.7	5.9	4.3	3.8	7.0	6.8	4.1	4.2					
7		0.054	0.044	0.040	0.058	0.052	0.030	0.044	0.044	0.054	0.042	0.050	0.046	0.054	0.040	0.027	0.050	0.048
		4.5	4.3	3.1	5.0	4.0	5.1	7.3	6.0	5.4	7.0	8.2	5.8	5.5	5.5	4.0	4.4	3.6
			0.052	0.054	0.060	0.054	0.030	0.060	0.050	0.056	0.048	0.058	0.058	0.056	0.040			
			3.6	4.7	5.0	6.1	6.0	8.0	7.3	4.2	6.0	7.4	7.7	5.8	3.7			
				0.066	0.060	0.058	0.030	0.064	0.054		0.054	0.062	0.060	0.056	0.052			
				5.5	6.0	5.2	7.7	7.7	7.2		6.1	7.3	5.7	6.1	4.9			
8	0.046	0.054	0.058	0.048	0.048	0.060	0.060	0.070	0.060	0.066	0.052	0.048	0.046	0.052	0.040	0.048	0.052	0.046
	4.0	4.1	3.6	3.7	4.0	6.1	7.4	6.7	5.0	7.5	6.0	5.0	7.7	4.7	4.0	4.4	3.1	4.0
		0.054		0.062	0.054	0.070	0.062	0.074	0.060	0.068	0.066	0.060	0.060	0.064	0.056	0.050	0.054	
		4.2		5.0	4.4	6.3	5.1	5.7	4.8	5.7	5.7	4.8	6.3	4.2	2.8	3.9	4.4	
					0.058		0.064	0.084	0.064	0.068	0.068	0.066	0.062	0.064	0.064	0.050		
					6.0		5.5	6.8	6.7	7.4	8.0	7.0	5.6	5.6	5.0	3.9		
9		0.070	0.070	0.068	0.074	0.056	0.066	0.064	0.076	0.074	0.070	0.068	0.078	0.060	0.060	0.062	0.052	0.064
		1.7	1.7	2.4	3.6	6.6	4.1	7.6	6.8	7.5	7.3	5.0	5.4	4.8	4.8	4.6	3.5	3.5
						0.066	0.076	0.074	0.082	0.076	0.080	0.076		0.062	0.080			
						6.0	4.5	4.6	6.8	5.0	7.5	3.5		4.8	3.8			
							0.076	0.082	0.086	0.080	0.098							
							4.5	4.7	6.2	6.5	5.5							
10		0.060	0.050	0.050	0.060	0.064	0.070	0.062	0.066	0.068	0.062	0.070	0.066	0.062	0.070	0.054	0.074	0.062
		2.5	3.8	4.0	5.7	5.5	6.0	4.6	6.0	6.6	7.1	6.1	4.0	6.5	3.2	5.0	4.8	2.5
			0.054	0.056	0.066	0.070	0.076	0.062	0.076	0.074	0.070	0.078	0.070	0.066	0.072	0.060		
			3.5	5.0	3.5	6.8	6.4	5.1	7.0	7.4	6.0	4.8	4.0	5.5	4.3	4.0		
			0.058	0.058	0.066	0.080	0.080		0.078	0.080	0.076	0.078	0.070	0.070	0.072			
			3.5	2.2	6.2	5.0	5.0		7.5	6.2	7.7	6.3	5.4	4.0	5.4			

TABLE I. - Concluded. DROP DIAMETERS AND RADIAL POSITIONS OF THREE LARGEST DROPS IN EACH SPRAY SECTOR OBTAINED FROM SHADOWGRAPH RECORDS

[Spray axis horizontal.]

35 millimeter picture frame	Drop diameter, in. / Distance from impingement point, in.																	
	Angular position, deg																	
	Above spray axis									Below spray axis								
	90	80	70	60	50	40	30	20	10	10	20	30	40	50	60	70	80	90
Jet velocity, 60 ft/sec																		
11	-----	0.052 / 4.3	0.050 / 2.8	0.044 / 3.6	0.064 / 3.3	0.048 / 7.8	0.058 / 6.6	0.054 / 5.3	0.042 / 7.0	0.040 / 6.0	0.046 / 6.5	0.046 / 7.3	0.046 / 4.4	0.050 / 5.3	0.052 / 3.1	0.050 / 3.8	0.048 / 3.1	0.052 / 3.4
	-----	-----	-----	0.050 / 3.5	-----	0.050 / 7.7	0.058 / 6.7	0.056 / 5.4	0.050 / 7.5	0.046 / 7.3	0.058 / 7.9	0.050 / 7.4	0.046 / 5.1	0.054 / 6.3	-----	-----	-----	-----
	-----	-----	-----	-----	-----	0.054 / 6.8	0.060 / 6.5	0.064 / 5.2	0.058 / 7.4	0.052 / 7.4	0.064 / 7.0	0.050 / 7.8	0.048 / 6.5	0.056 / 4.3	-----	-----	-----	-----
12	0.062 / 2.7	-----	0.062 / 2.8	0.060 / 3.1	0.058 / 5.3	0.074 / 3.8	0.062 / 4.6	0.052 / 7.7	0.058 / 7.1	0.066 / 6.6	0.060 / 7.1	0.052 / 5.6	0.054 / 4.8	0.048 / 5.5	0.066 / 3.0	0.052 / 3.0	0.056 / 2.1	-----
	-----	-----	-----	-----	0.062 / 3.3	0.074 / 4.7	0.070 / 4.8	0.068 / 4.6	0.076 / 5.5	0.068 / 7.7	0.070 / 7.3	0.064 / 6.4	0.062 / 5.4	0.066 / 4.0	-----	-----	0.056 / 3.4	-----
	-----	-----	-----	-----	-----	-----	-----	0.070 / 7.8	0.088 / 6.5	0.074 / 4.4	0.078 / 6.4	0.064 / 6.7	0.062 / 7.0	-----	-----	-----	-----	-----
13	-----	0.060 / 3.7	0.060 / 2.5	0.064 / 3.5	0.060 / 3.4	0.060 / 5.4	0.054 / 6.4	0.040 / 4.7	0.058 / 7.3	0.046 / 5.1	0.044 / 7.3	0.040 / 8.3	0.056 / 5.5	0.052 / 4.0	0.050 / 5.5	-----	-----	-----
	-----	-----	-----	-----	0.060 / 3.6	0.066 / 5.5	0.056 / 3.8	0.044 / 5.3	0.060 / 5.8	0.052 / 7.5	0.050 / 7.3	0.056 / 8.1	0.056 / 6.6	0.056 / 5.5	0.056 / 3.5	-----	-----	-----
	-----	-----	-----	-----	-----	-----	0.060 / 6.9	0.066 / 5.6	0.066 / 5.2	0.064 / 7.0	0.058 / 5.5	0.064 / 6.1	0.062 / 5.4	0.060 / 4.5	0.070 / 5.8	-----	-----	-----
14	0.062 / 2.6	-----	-----	0.052 / 2.8	0.072 / 4.3	0.072 / 5.1	0.064 / 5.5	0.064 / 3.0	0.066 / 3.5	0.060 / 5.1	0.056 / 7.5	0.064 / 7.2	0.050 / 5.7	0.060 / 4.3	0.066 / 4.6	0.052 / 3.2	0.072 / 4.3	-----
	-----	-----	-----	0.058 / 2.2	0.076 / 3.0	0.080 / 6.2	0.070 / 6.0	0.068 / 7.4	0.068 / 4.8	0.062 / 4.7	0.062 / 4.6	0.064 / 8.3	0.062 / 5.0	0.070 / 5.7	-----	0.060 / 4.5	-----	-----
	-----	-----	-----	-----	-----	-----	0.076 / 6.8	0.090 / 6.2	0.068 / 5.3	0.070 / 7.5	0.064 / 4.6	-----	-----	-----	-----	-----	-----	-----
15	-----	-----	-----	0.060 / 1.8	0.060 / 2.5	0.050 / 3.6	0.062 / 3.5	0.060 / 5.0	0.060 / 7.3	0.060 / 7.6	0.070 / 6.5	0.066 / 6.7	0.056 / 6.1	0.070 / 2.8	0.066 / 4.5	0.062 / 3.2	0.044 / 2.5	0.050 / 2.8
	-----	-----	-----	-----	0.070 / 4.0	0.062 / 3.5	0.072 / 6.0	0.066 / 6.8	0.064 / 7.4	0.066 / 6.8	0.072 / 6.7	0.072 / 6.0	0.060 / 7.2	0.072 / 6.0	0.070 / 4.2	-----	0.052 / 3.5	-----
	-----	-----	-----	-----	-----	-----	0.080 / 6.0	0.076 / 4.2	0.080 / 7.0	0.070 / 5.6	0.072 / 7.0	-----	0.068 / 4.6	0.076 / 4.2	-----	-----	-----	-----
Jet velocity, 74 ft/sec																		
16	-----	0.070 / 4.8	0.054 / 2.6	0.066 / 3.3	0.068 / 6.3	0.060 / 6.5	0.062 / 3.4	0.062 / 5.1	0.070 / 6.0	0.076 / 7.4	0.056 / 8.0	0.062 / 8.0	0.062 / 7.0	0.054 / 5.5	0.062 / 3.1	0.062 / 2.8	0.068 / 2.6	0.076 / 2.0
	-----	-----	-----	-----	0.072 / 4.2	-----	0.064 / 7.1	0.066 / 4.0	0.070 / 6.0	0.082 / 5.2	0.070 / 6.0	0.070 / 7.2	0.062 / 7.0	0.058 / 4.8	0.074 / 5.0	0.074 / 3.0	-----	0.076 / 2.3
	-----	-----	-----	-----	-----	-----	0.074 / 7.3	0.068 / 4.3	0.076 / 5.6	0.084 / 6.0	0.070 / 8.0	0.086 / 4.8	0.062 / 7.0	0.066 / 3.4	-----	-----	-----	-----
17	-----	-----	-----	-----	0.040 / 5.8	0.044 / 5.3	0.050 / 4.6	0.044 / 4.7	0.042 / 7.6	0.042 / 7.7	0.042 / 4.5	0.044 / 4.4	0.036 / 5.5	0.040 / 5.4	0.042 / 3.9	0.044 / 2.8	0.050 / 3.7	0.042 / 4.5
	-----	-----	-----	-----	-----	0.046 / 5.2	0.058 / 3.8	0.048 / 5.8	0.048 / 6.0	0.044 / 4.4	0.048 / 5.6	0.044 / 7.8	0.040 / 8.3	0.042 / 4.3	0.052 / 4.2	0.044 / 3.5	-----	0.054 / 3.4
	-----	-----	-----	-----	-----	0.048 / 3.8	0.060 / 5.3	0.060 / 5.5	0.056 / 6.0	0.046 / 4.6	0.054 / 6.8	0.050 / 7.6	0.046 / 6.3	0.054 / 4.3	0.054 / 5.5	-----	-----	0.078 / 4.0
18	-----	0.044 / 2.8	-----	0.056 / 2.8	0.050 / 3.3	0.040 / 5.6	0.042 / 4.5	0.046 / 4.2	0.036 / 5.6	0.042 / 4.3	0.040 / 7.8	0.042 / 7.7	0.050 / 6.7	0.046 / 4.2	0.048 / 3.5	0.042 / 2.9	0.042 / 4.4	0.050 / 4.5
	-----	-----	-----	-----	0.058 / 1.8	0.046 / 2.6	0.048 / 4.1	0.050 / 4.6	0.052 / 5.6	0.048 / 4.8	0.052 / 7.4	0.044 / 6.1	0.050 / 6.8	0.046 / 4.6	0.048 / 3.6	-----	0.064 / 4.0	0.052 / 3.6
	-----	-----	-----	-----	-----	-----	0.050 / 4.6	0.058 / 4.6	0.060 / 7.1	0.050 / 8.0	0.054 / 5.6	0.044 / 7.0	0.054 / 7.1	0.054 / 5.6	0.048 / 4.4	-----	-----	-----
19	-----	-----	-----	-----	0.046 / 6.0	0.060 / 6.0	0.050 / 4.5	0.044 / 5.0	0.046 / 7.6	0.040 / 6.0	0.044 / 7.5	0.046 / 7.0	0.048 / 7.4	0.048 / 3.6	0.042 / 4.7	0.048 / 2.7	0.052 / 1.7	0.044 / 0.16
	-----	-----	-----	-----	0.056 / 3.3	-----	0.052 / 4.0	0.052 / 7.1	0.056 / 5.4	0.040 / 7.5	0.050 / 4.7	0.050 / 6.3	0.050 / 4.8	0.050 / 4.0	-----	0.052 / 4.3	-----	-----
	-----	-----	-----	-----	-----	-----	0.060 / 4.2	0.058 / 7.9	-----	0.044 / 6.8	0.058 / 6.3	0.050 / 7.0	0.050 / 5.5	-----	-----	-----	-----	-----
20	-----	-----	-----	-----	-----	0.048 / 3.8	0.052 / 3.7	0.048 / 4.3	0.050 / 4.6	0.050 / 7.7	0.048 / 7.3	0.048 / 8.1	0.040 / 7.3	0.044 / 5.7	0.056 / 4.0	0.044 / 4.8	0.042 / 4.0	0.060 / 4.0
	-----	-----	-----	-----	-----	0.060 / 3.5	0.058 / 5.2	0.052 / 7.3	0.050 / 6.7	0.052 / 6.6	0.052 / 5.0	0.048 / 8.1	0.046 / 7.5	0.058 / 3.5	0.056 / 4.5	0.048 / 3.8	0.048 / 2.4	-----
	-----	-----	-----	-----	-----	-----	0.062 / 4.5	0.062 / 7.6	0.052 / 5.9	0.054 / 7.7	0.056 / 5.4	0.056 / 8.0	0.052 / 5.7	0.060 / 4.4	0.056 / 4.0	-----	-----	-----

TABLE II. - DROP DATA FOR LATERAL DISTANCE SAMPLING

Drop diameter, microns	Lateral distance, in.						
	0	1	2	3	4	5	6
	Number of drops						
50	55	56	60	100	70	--	--
100	35	38	26	60	20	42	30
125	13	--	--	--	--	--	--
150	9	28	17	20	--	13	--
200	7	15	12	9	10	7	17
250	6	--	--	--	8	--	11
300	5	10	8	7	7	5	8
350	--	--	--	--	--	--	--
400	4	8	7	6	5	4	5
500	3	6	6	4	4	2	3
600	2	--	3	--	2	1	2
700	1	5	2	--	--	1	--
800	--	4	1	--	--	1	--
900	--	--	1	--	--	--	--

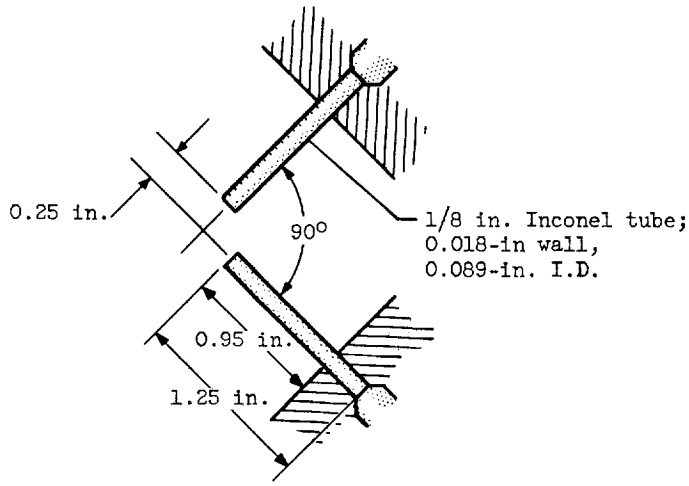

(a) Atomizer detail.

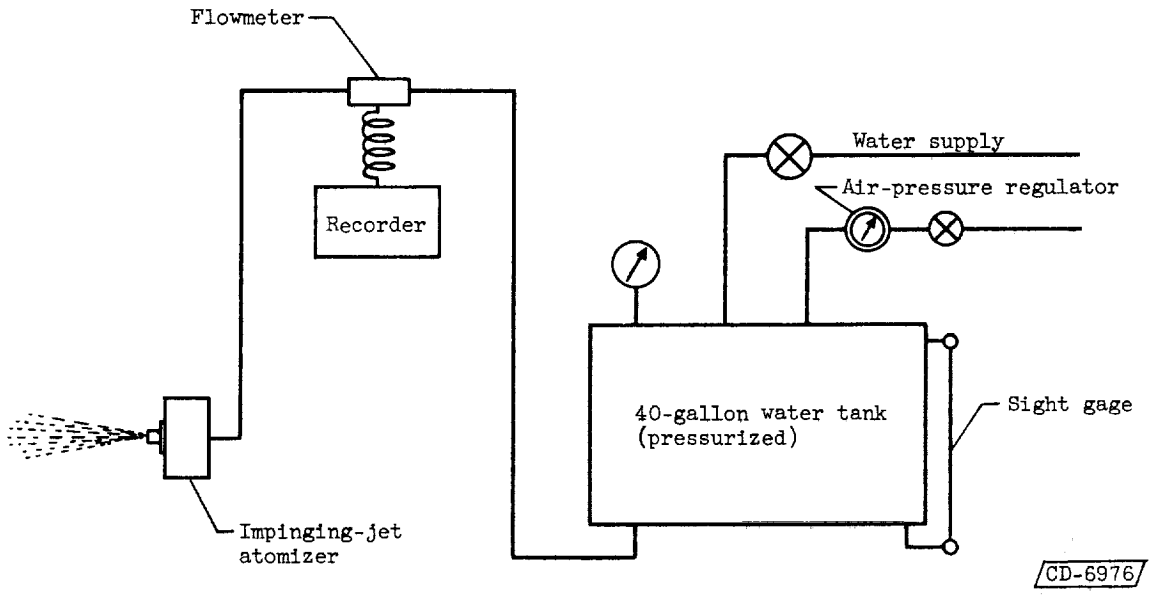

(b) Flow apparatus.

Figure 1. - Schematic diagrams of impinging-jet and photography apparatus.

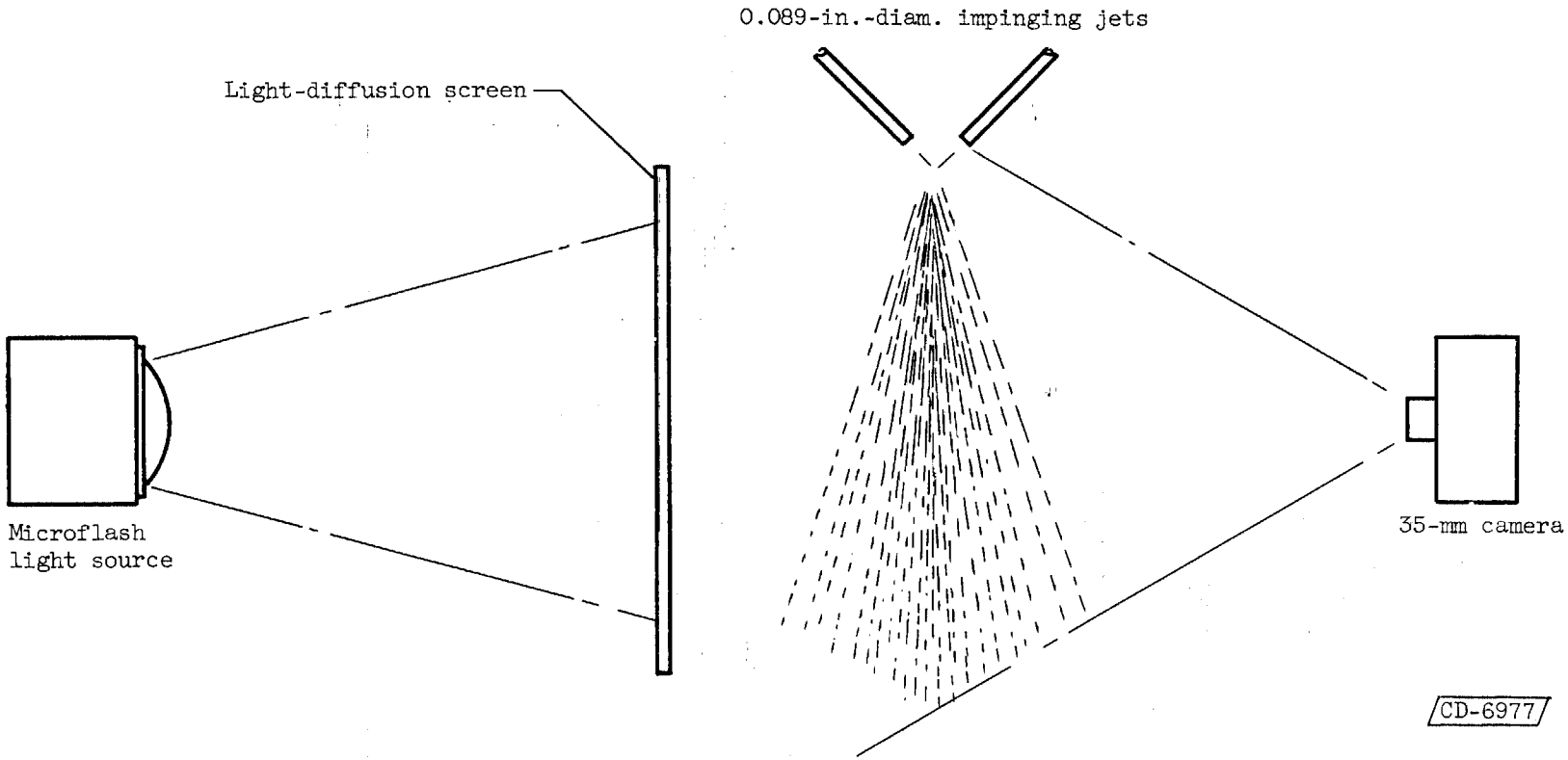

(c) Apparatus for shadowgraphs of spray patterns (e.g., fig. 2).

Figure 1. - Continued. Schematic diagrams of impinging-jet and photography apparatus.

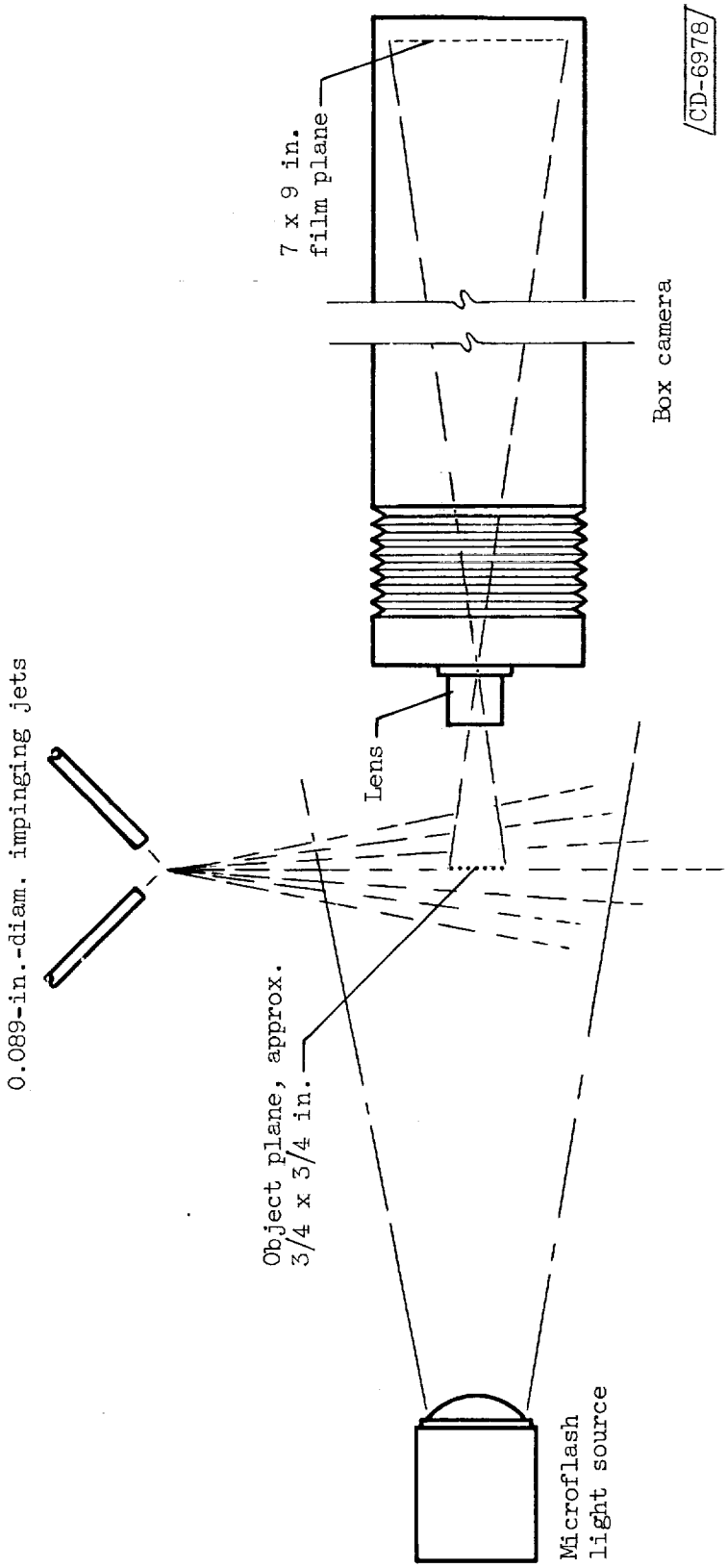

(d) Apparatus for photomicrographs; magnification, approximately 8.5.

Figure 1. - Continued. Schematic diagrams of impinging-jet and photography apparatus.

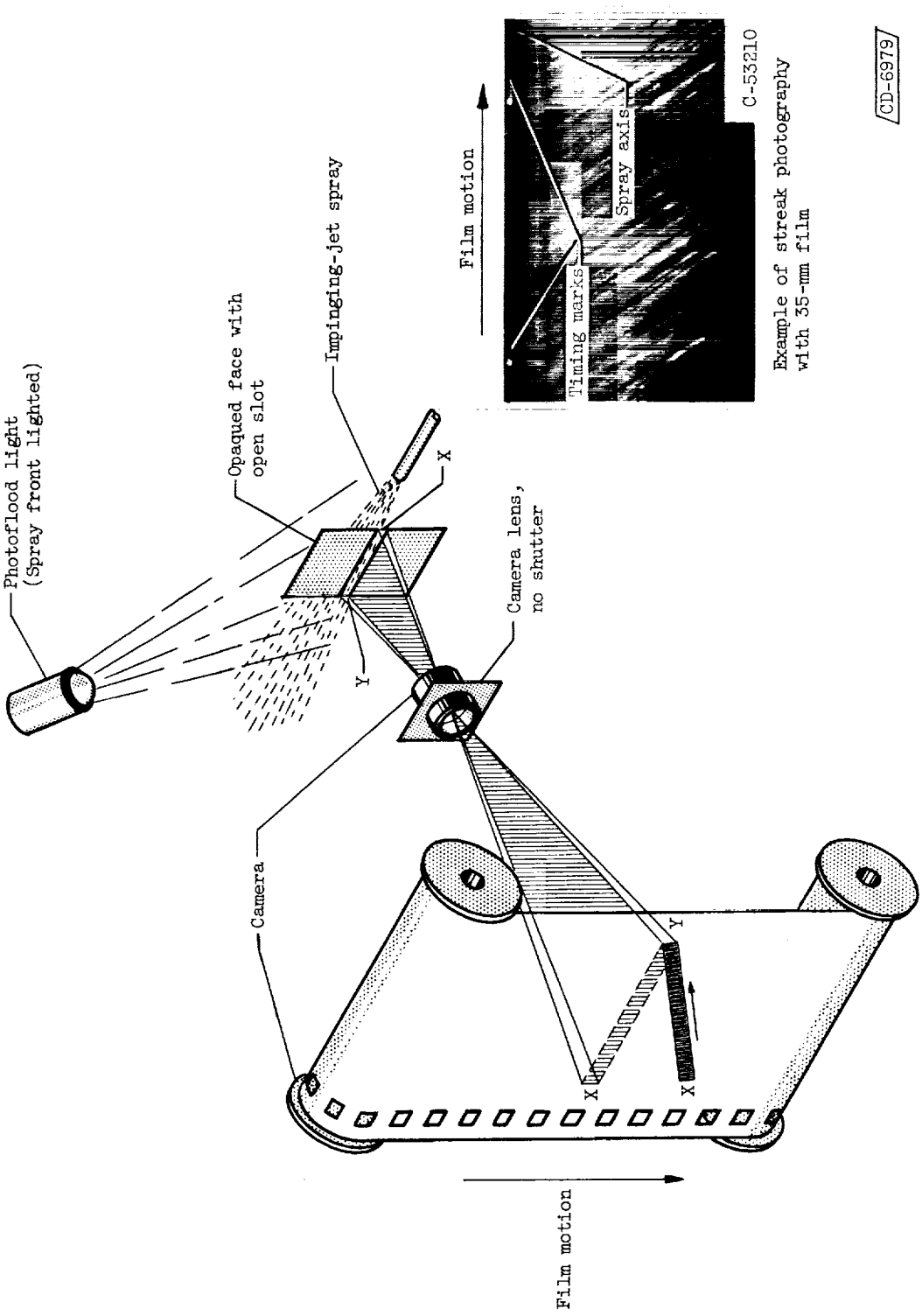

(e) Apparatus for streak photography.

Figure 1. - Continued. Schematic diagrams of impinging-jet and photography apparatus.

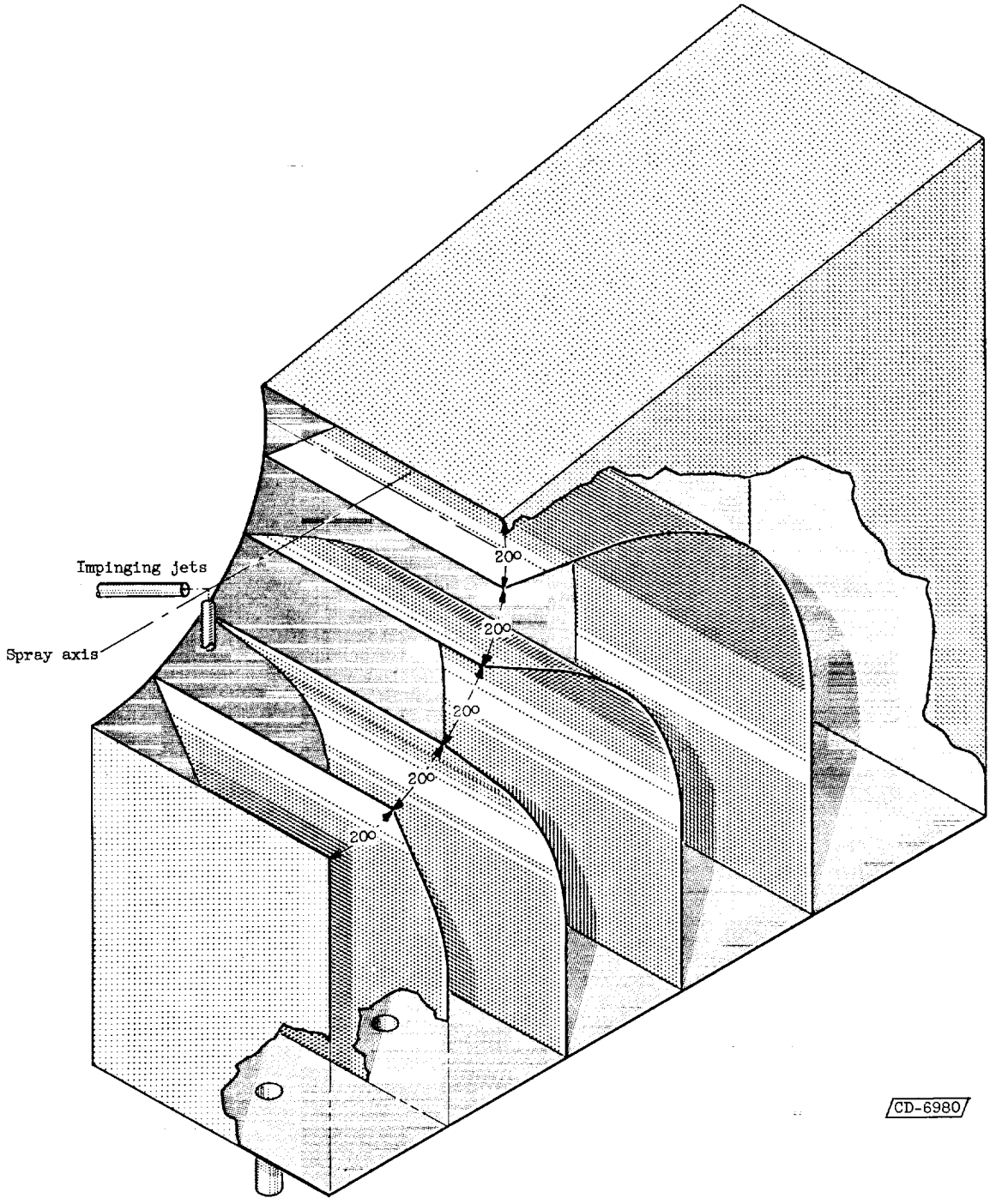

(f) Spray collector.

Figure 1. - Concluded. Schematic diagrams of impinging-jet and photography apparatus.

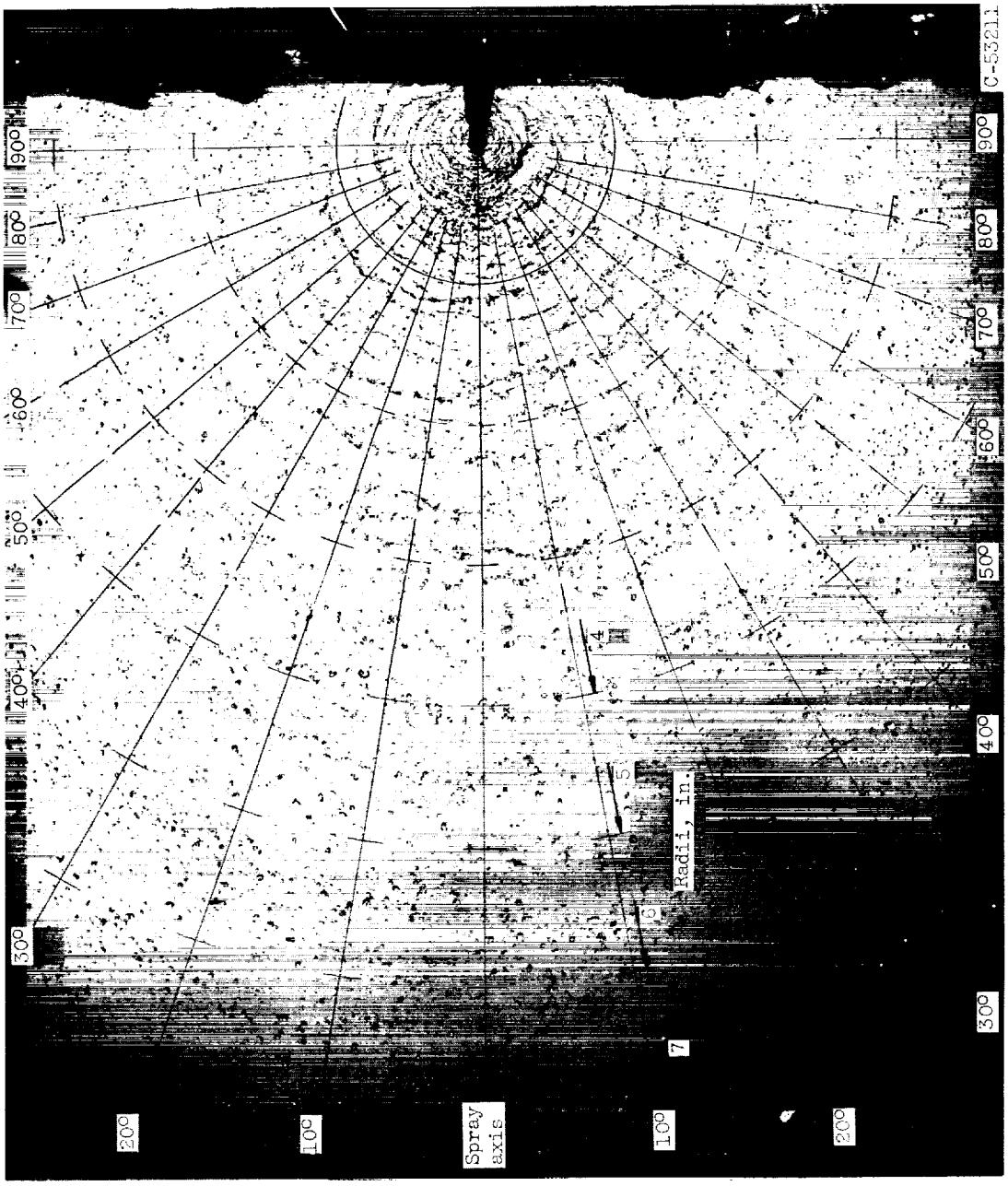

Figure 2. - Example of photographic layout for spray analysis.

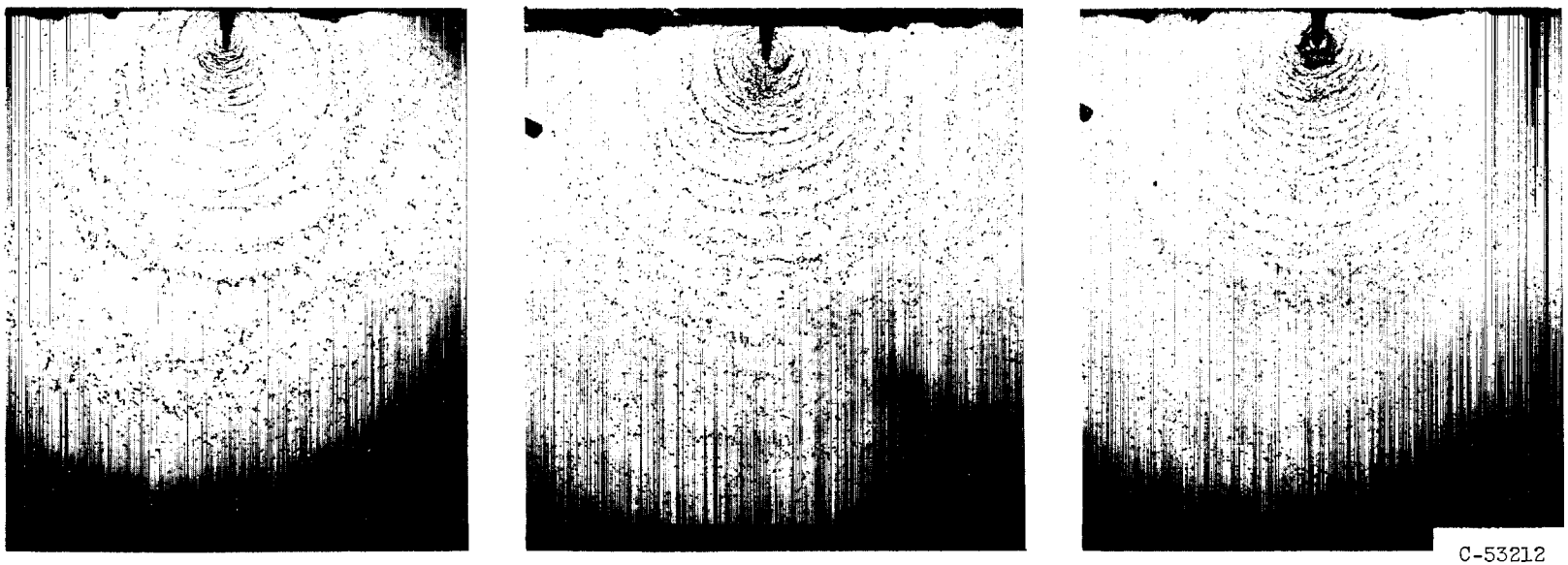

(a) Jet velocity, 30 feet per second. (b) Jet velocity, 60 feet per second. (c) Jet velocity, 74 feet per second.

Figure 3. - Free sprays from two impinging water jets at several jet velocities viewed paralled to plane of jets. Orifice diameter, 0.089 inch.

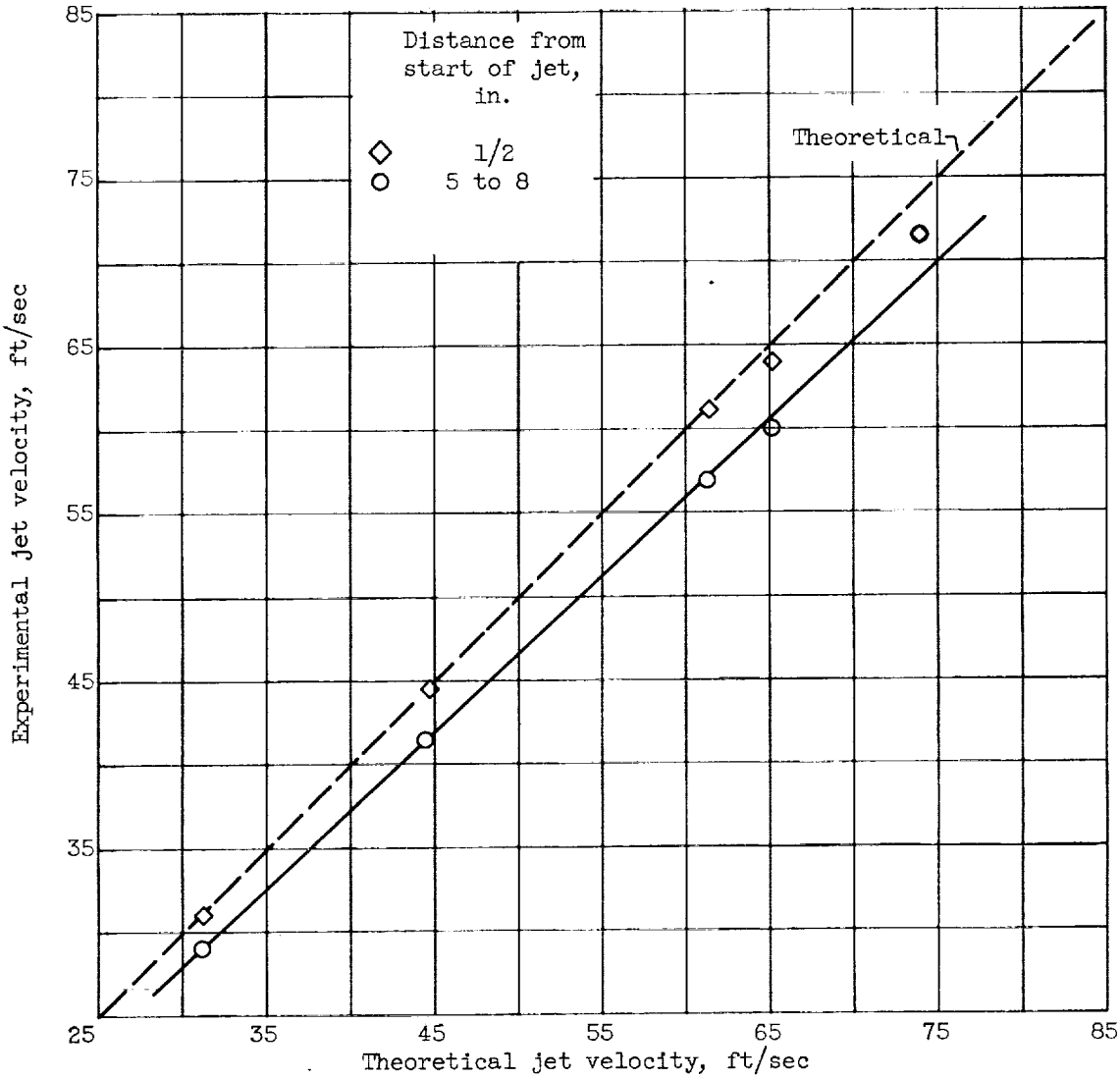

Figure 4. - Comparison of streak-photography and theoretical jet velocities.

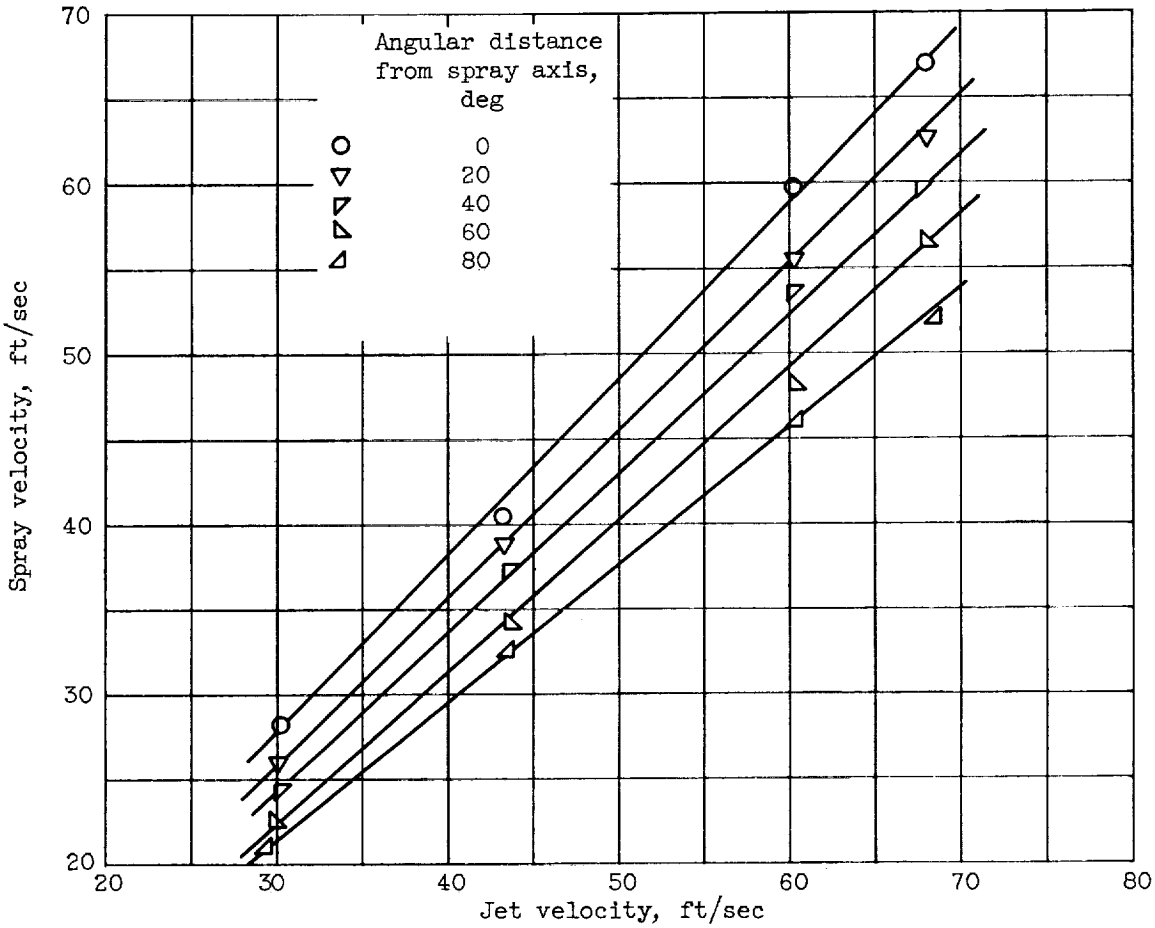

Figure 5. - Effect of jet velocity on spray velocity at different angular positions in spray plane. Distance from atomizer, 3 to 4 inches.

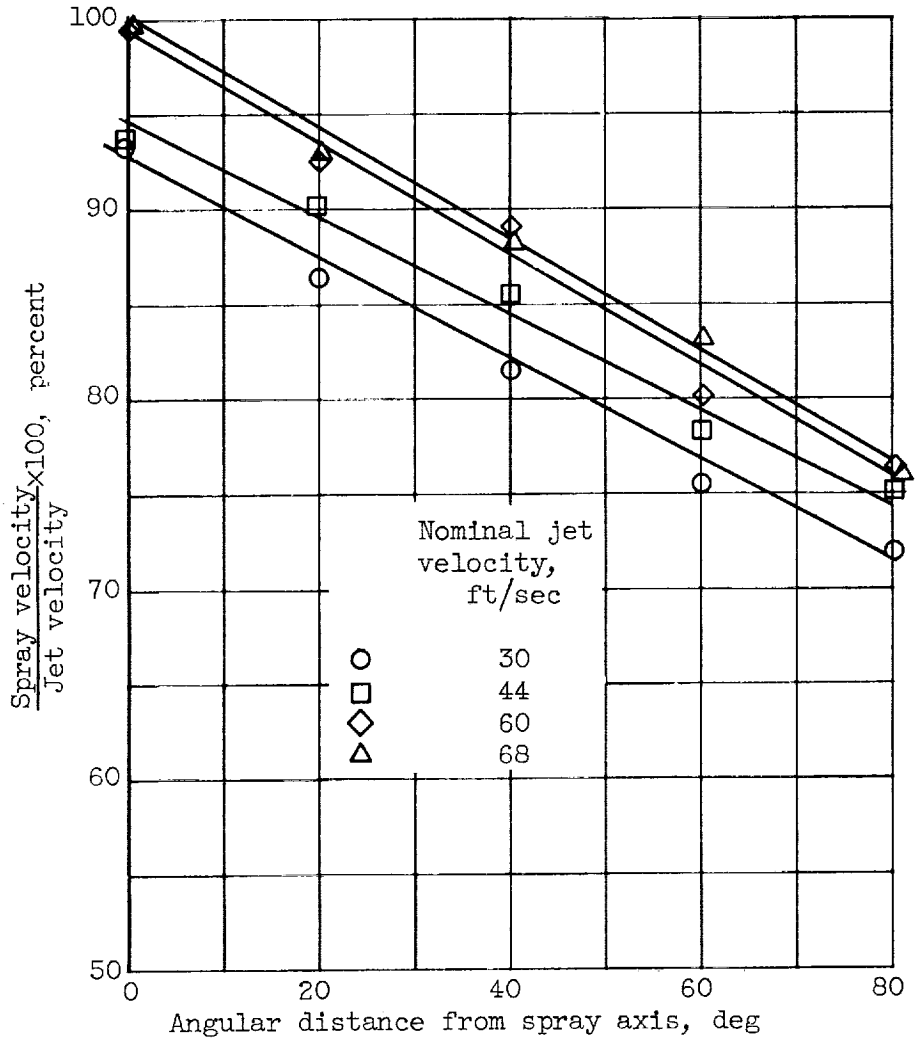

Figure 6. - Variation of ratio of spray velocity to jet velocity at different angular positions about spray axis for several jet velocities. Distance from atomizer, 3 to 4 inches.

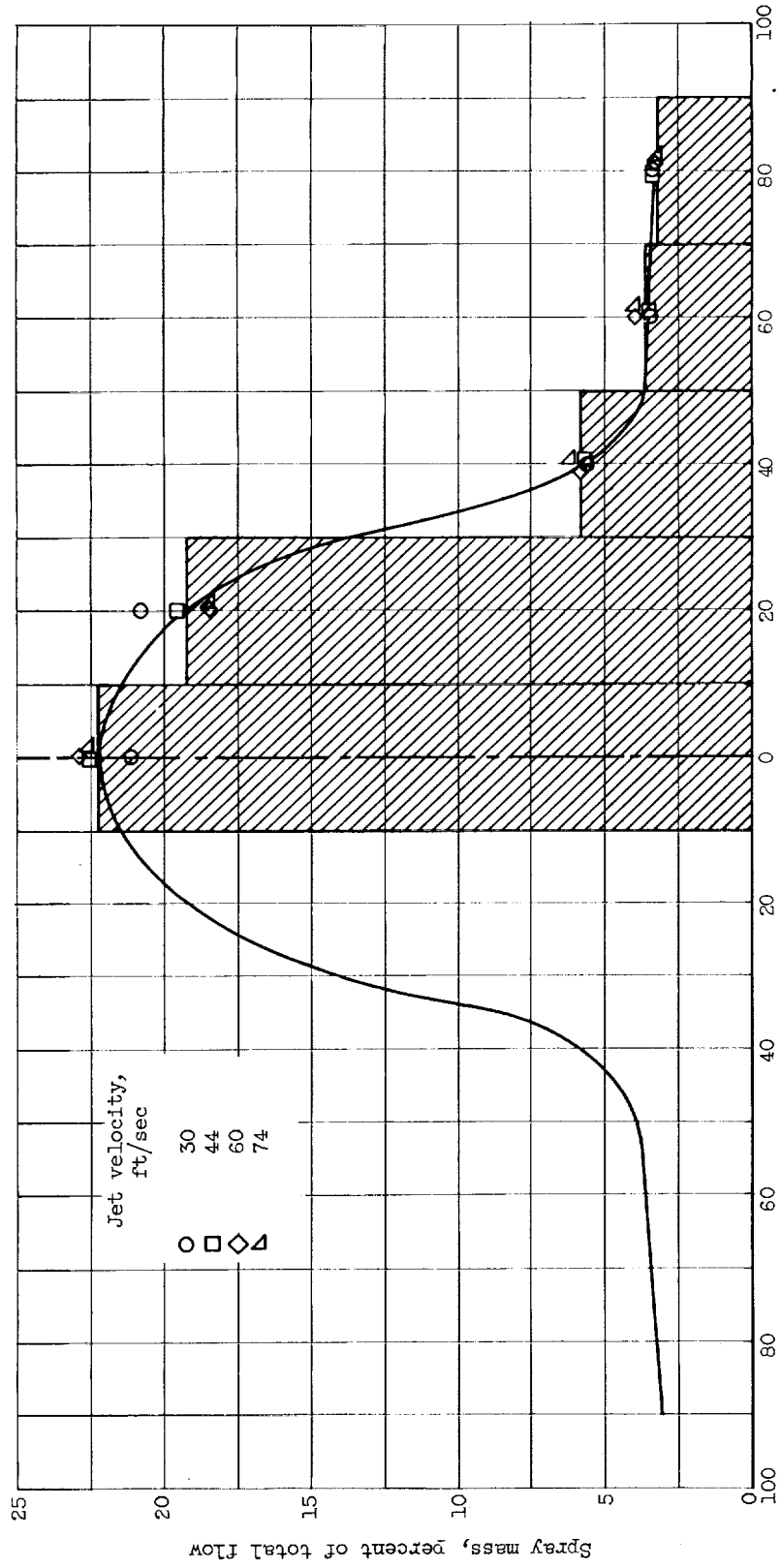

Figure 7. - Angular mass distribution of spray as determined from spray collection.

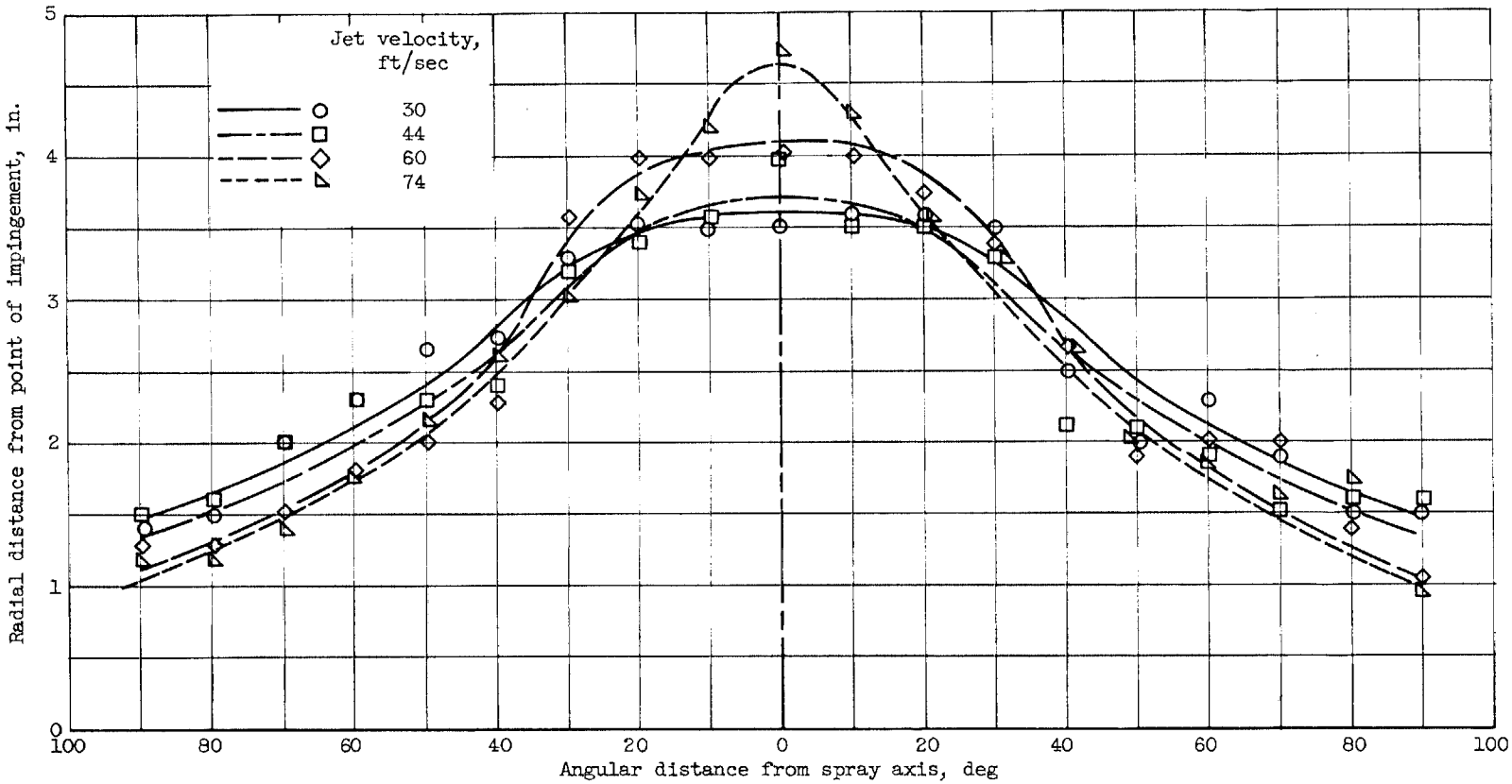

Figure 8. - Distance from point of jet impingement to breakup of ligaments into drops. Length of unbroken liquid sheet is equal to about one-half of values shown.

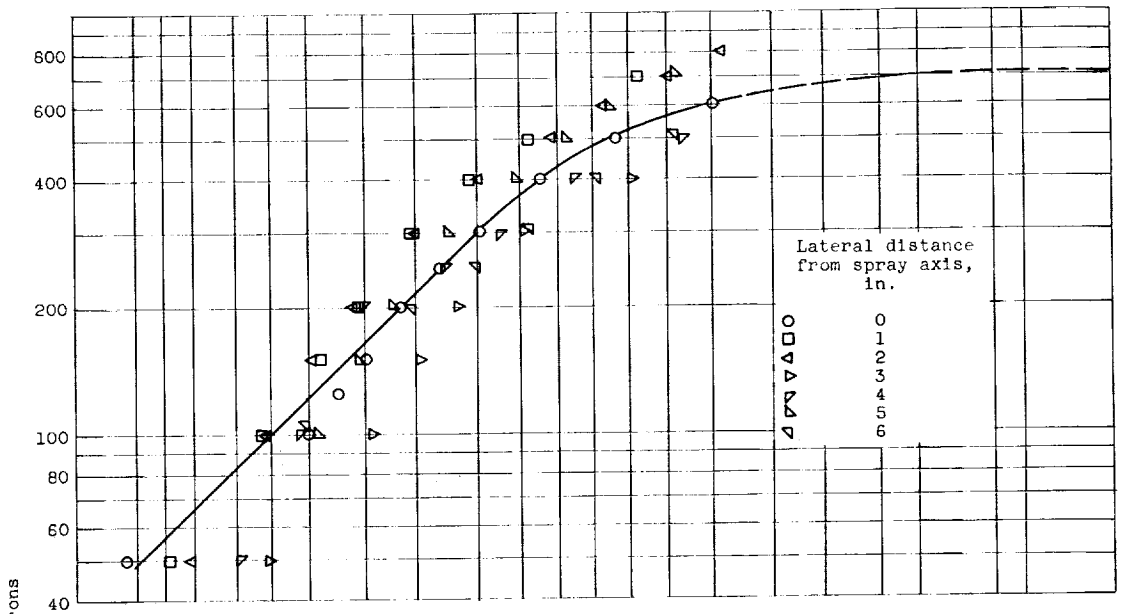

(a) Data from photomicrographs of present investigation. Jet velocity, 56 feet per second.

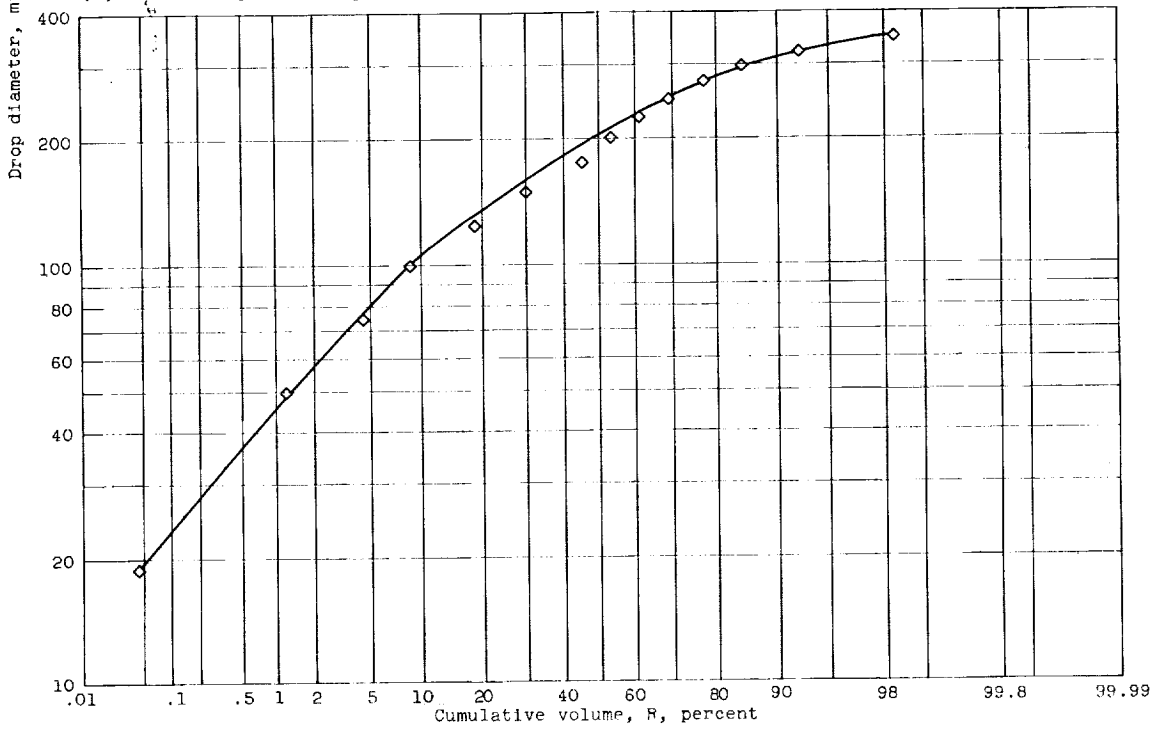

(b) Data from run 13 of reference 1. Jet velocity, 65 feet per second; airstream velocity, 180 feet per second.

Figure 9. - Log probability of atomization of impinging jets. Distance from atomizer, 8 inches; orifice diameter, 0.089 inch.

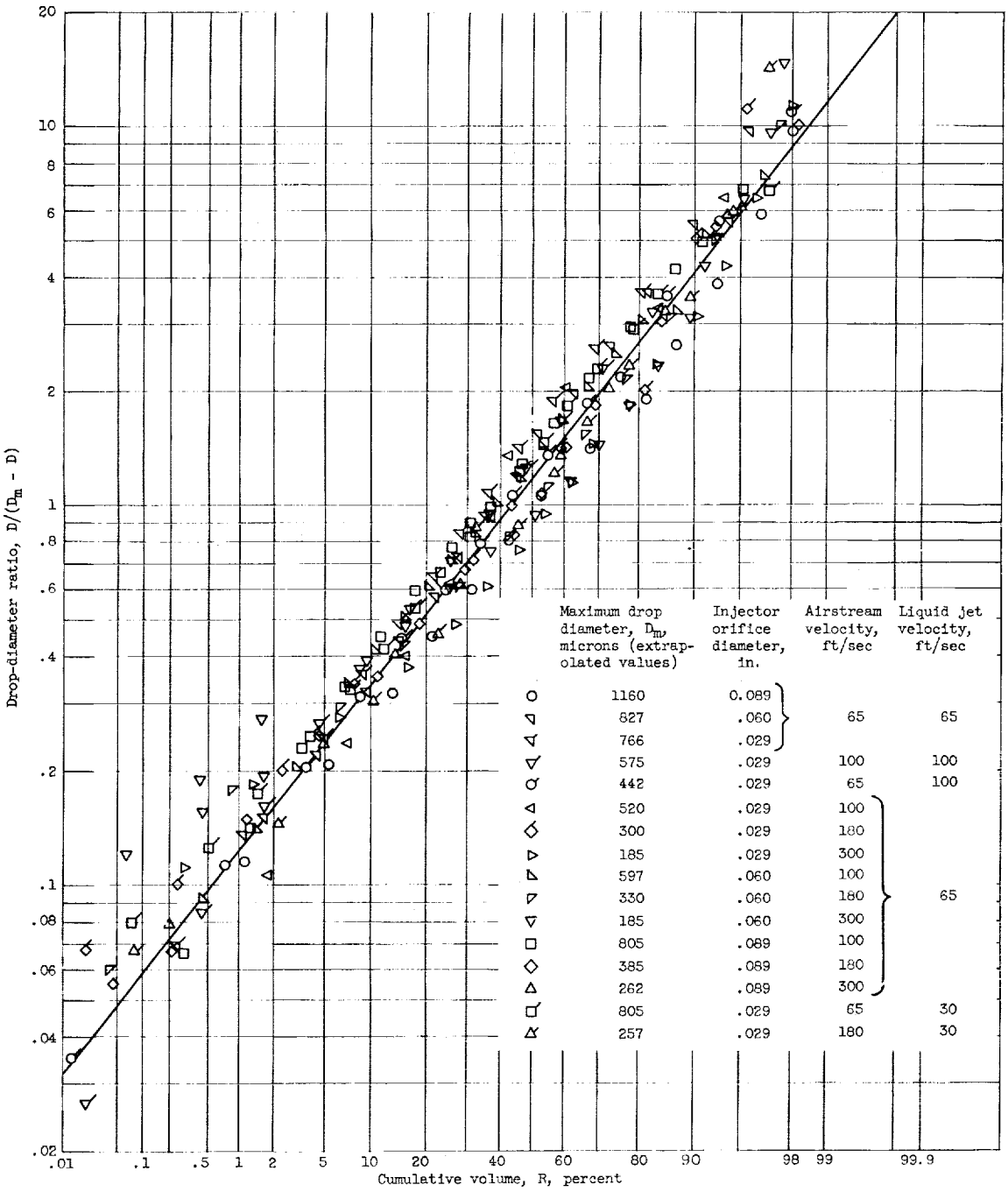

(a) From reference 1 (impinging heptane jets).

Figure 10. - "Upper-limit" analysis of drop-size distribution.

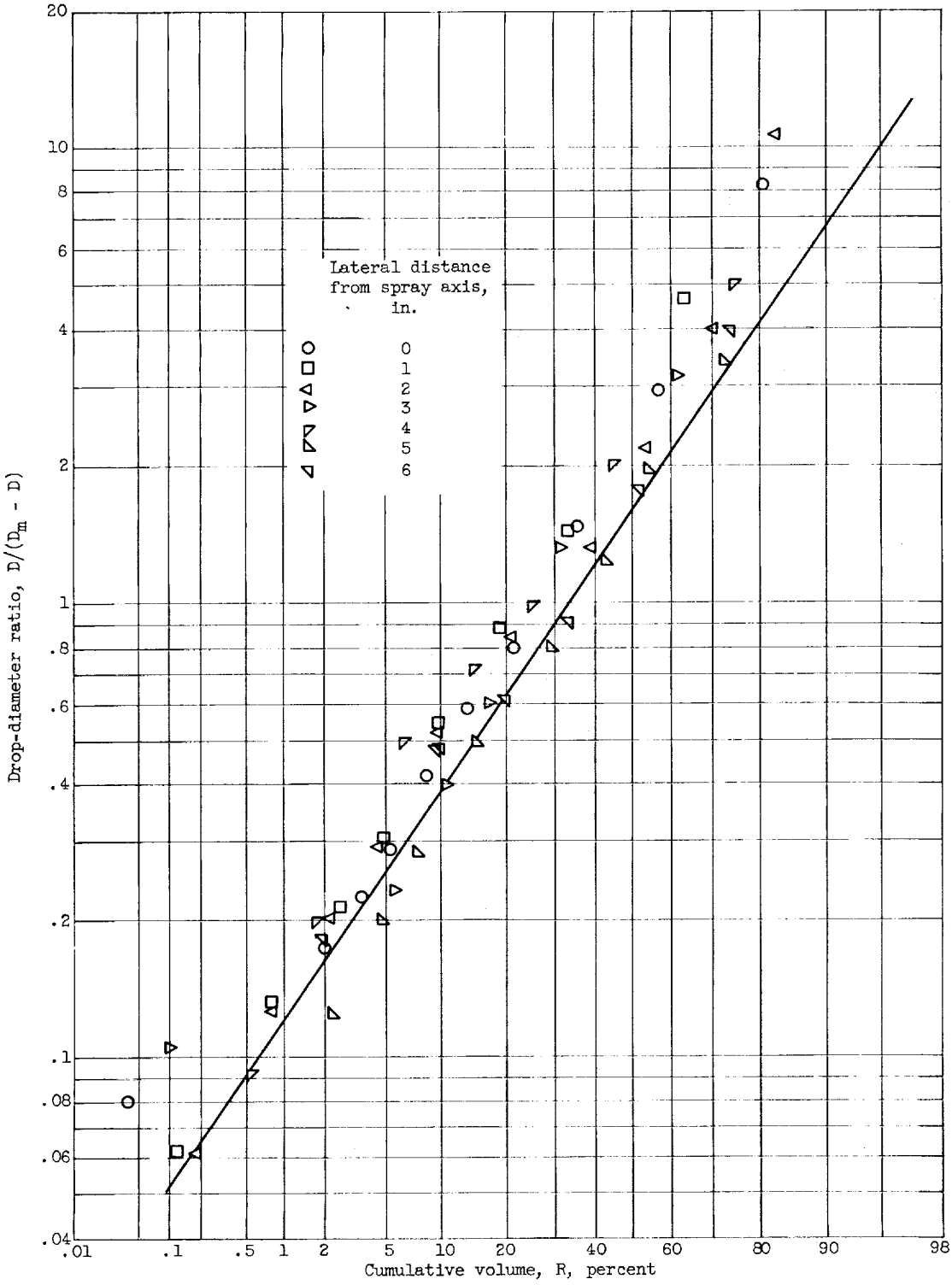

(b) From present investigation. Water jet velocity, 60 feet per second; jet diameter, 0.089 inch; distance downstream from atomizer, 8 inches.

Figure 10. - Concluded. "Upper-limit" analysis of drop-size distribution.

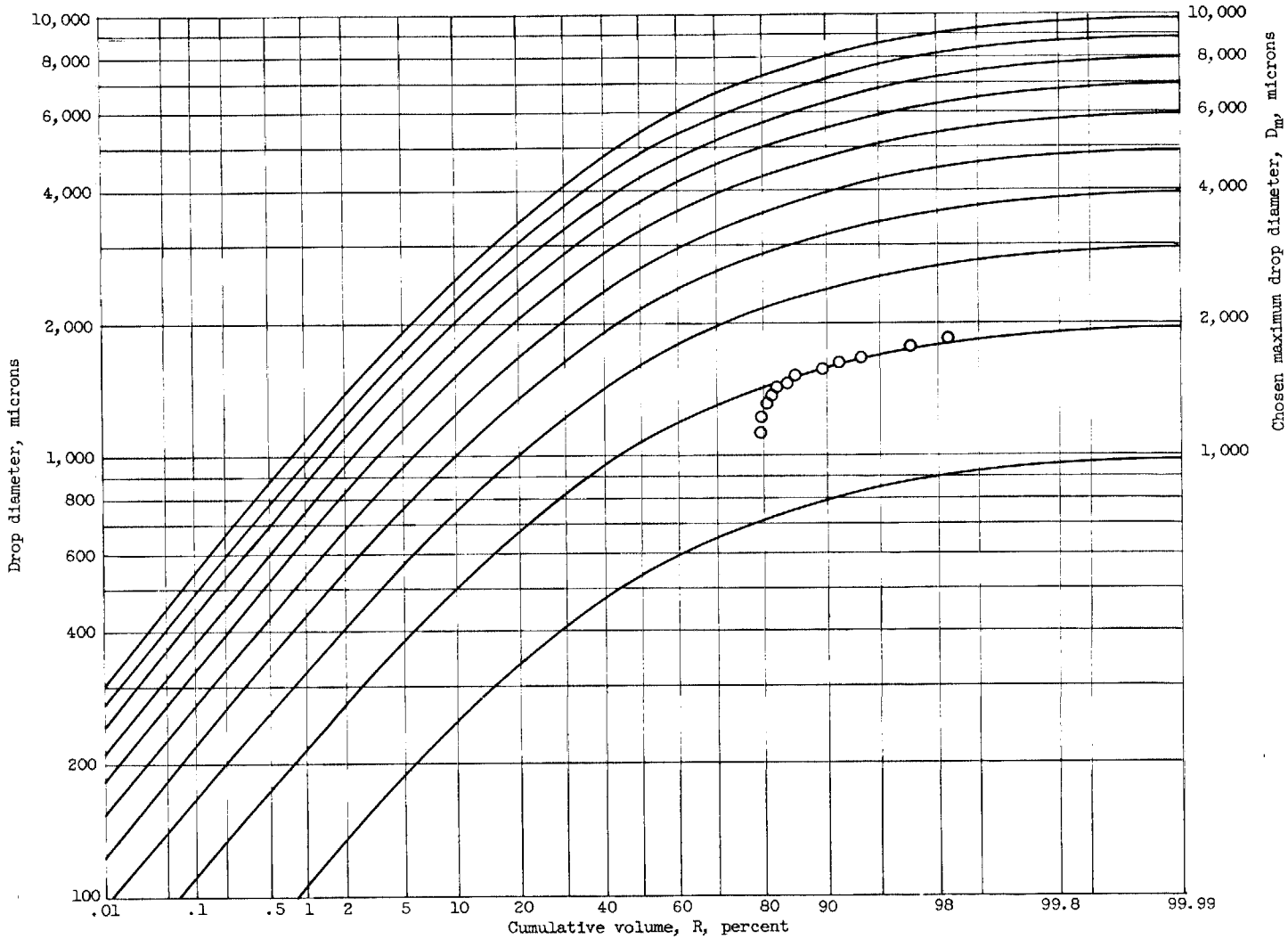

Figure 11. - Theoretical logarithmic normal curves prepared from relation shown in figure 10(a) for range of chosen values of maximum diameter (solid lines) and example of plotted values of partial distributions from large-drop sampling for water jet velocity of 44 feet per second and 50° angular position about spray axis (data points).

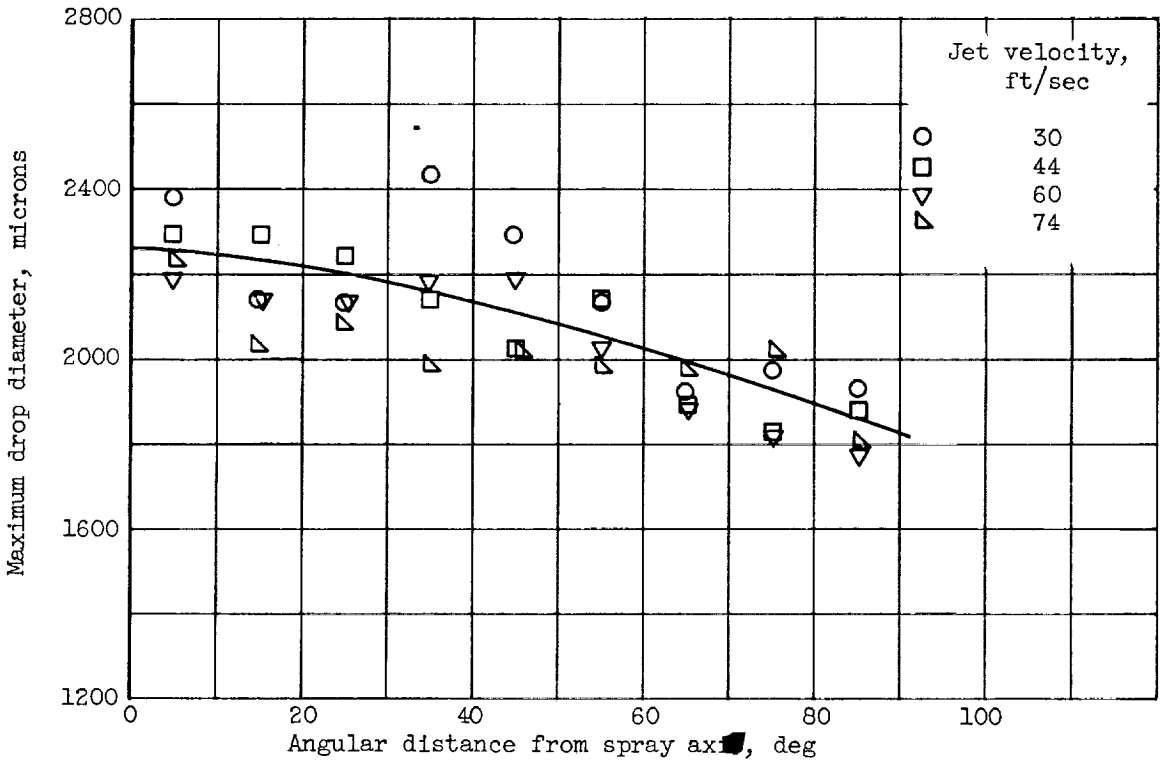

Figure 12. - Variation in extrapolated values of maximum drop diameter with angular position about spray axis for various jet velocities.

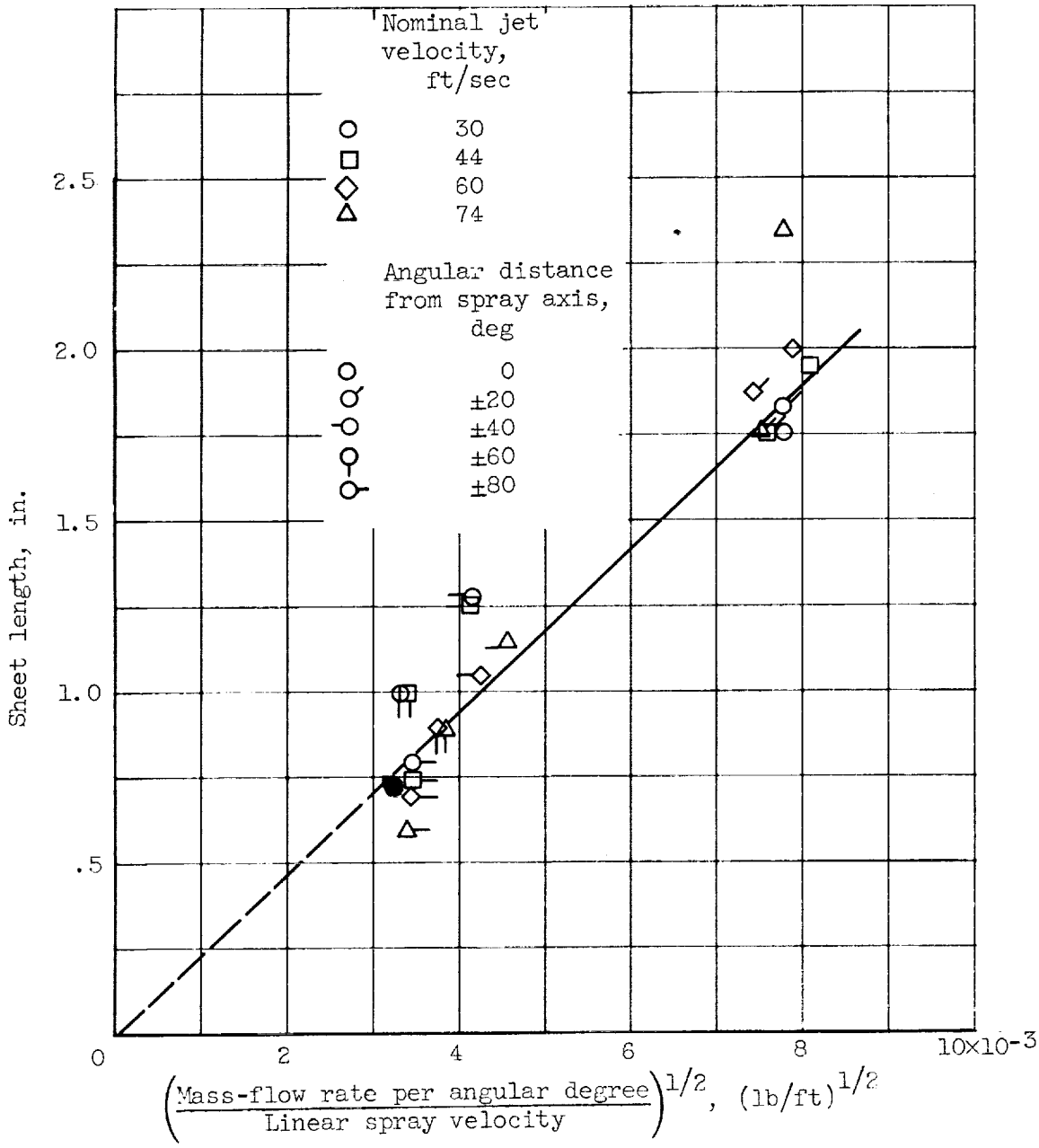

Figure 13. - Sheet length as function of ratio of mass-flow rate to spray velocity for several jet velocities and angular positions.

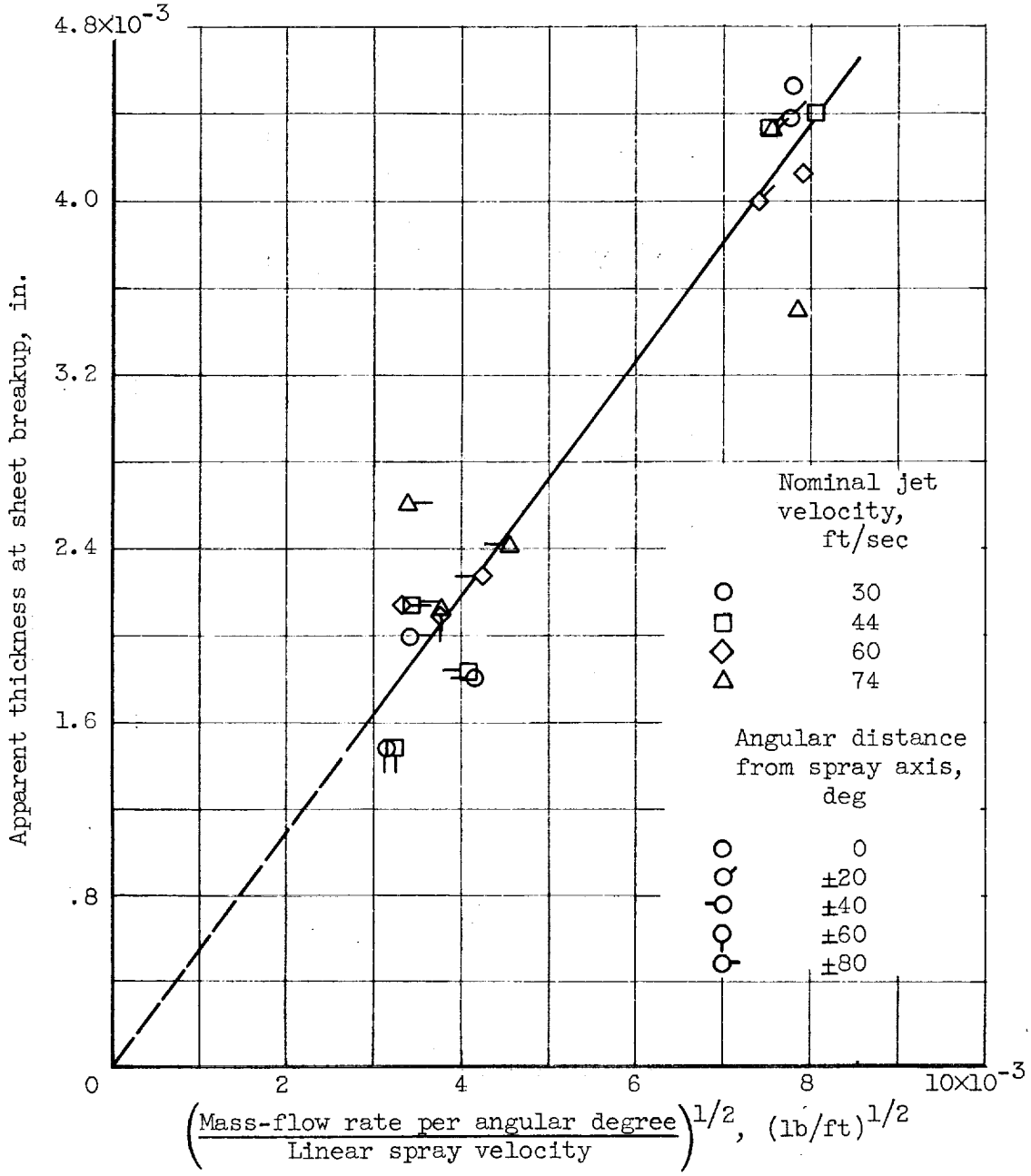

Figure 14. - Apparent sheet thickness at breakup as function of ratio of mass-flow rate to spray velocity for several jet velocities and angular positions.

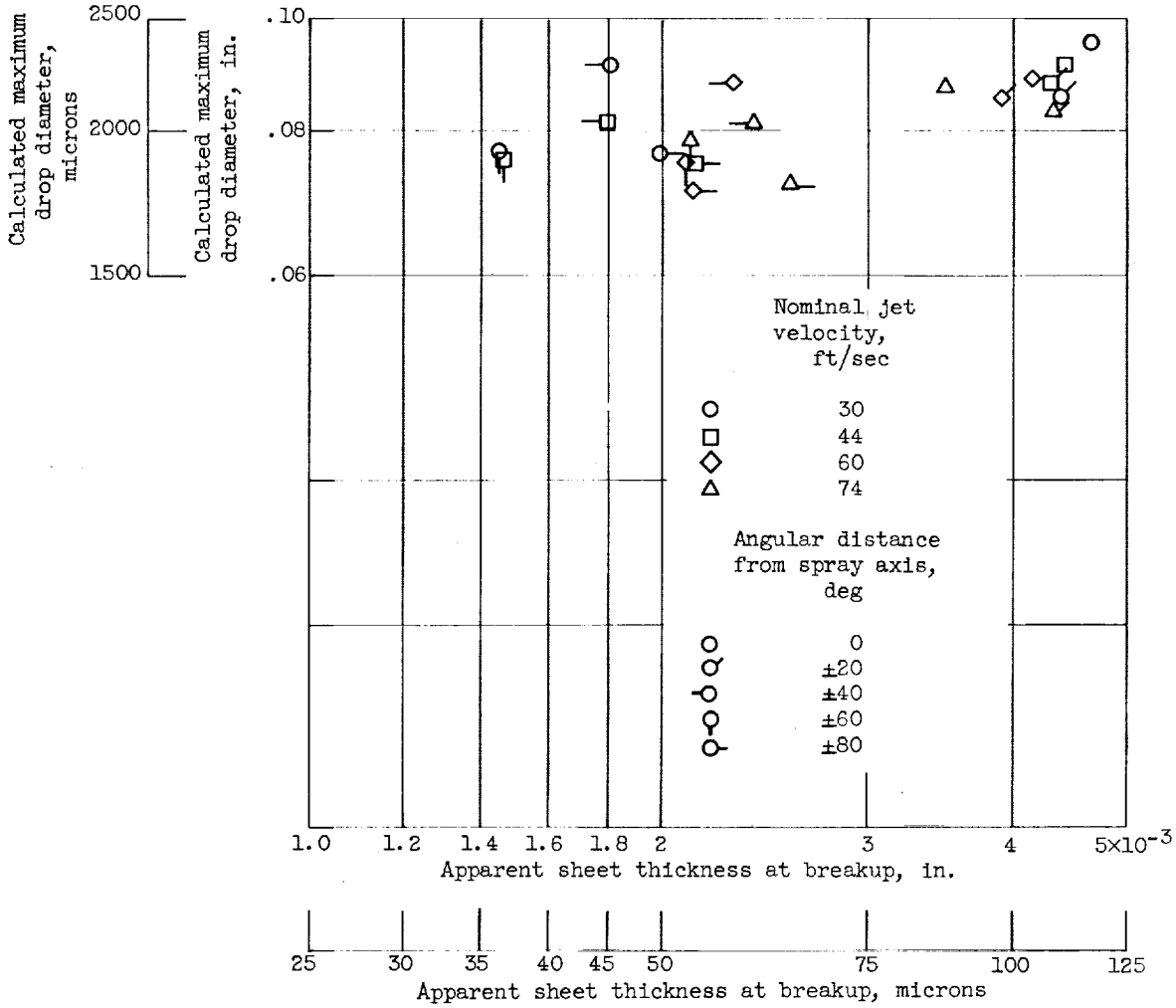

Figure 15. - Maximum drop diameter as function of apparent sheet thickness at breakup.

E-419